Available online at www.sciencedirect.com
SCIENCE DIRECT®
Optics Communications 222 (2003) 29–50
OPTICS COMMUNICATIONS
www.elsevier.com/locate/optcom

Origins of decoherence in coherent X-ray diffraction experiments

I.A. Vartanyants*,[1], I.K. Robinson

Department of Physics, University of Illinois, 1110 W. Green St., Urbana IL 61801, USA

Received 17 March 2003; received in revised form 12 May 2003; accepted 13 May 2003

Abstract

The propagation of the mutual intensity function from an incoherent synchrotron source to the sample is discussed. It is shown how coherency properties of the beam are changed by propagation through random optical elements, such as Be windows and mirrors present in the beamline. The mutual intensity function in this case cannot be described by one coherence length but will rather have several components with different coherence lengths. With computer simulations it is shown how such multicomponent mutual intensity function can affect the reconstruction of nanoparticles in coherent X-ray diffraction experiments.

PACS: 61.10.Dp; 41.50.+h; 42.30.Rx; 81.07.Bc

Keywords: Propagation of coherence; Coherent X-ray diffraction; Phase retrieval

1. Introduction

Current advances in experimental facilities (ESRF, APS, and SPRING-8) provide high-energy, high-brightness hard X-ray beams with relatively high degrees of coherence. The X-ray coherence lengths achievable with these latest synchrotron radiation sources are in the range of a few microns. The unique properties of these modern synchrotron sources have the potential to open new fields in X-ray physics such as fluctuation correlation dynamics [1–6], phase imaging [7–10], and coherent X-ray diffraction (CXD) [11–14]. All these techniques utilize the coherency properties of the synchrotron radiation [15].

As was shown in recent CXD experiments [16], it is possible to image crystals of nanometer size. Illuminated by coherent beam with transverse and longitudinal coherence lengths bigger than the size of the particle they produce a continuous interference diffraction pattern. The diffraction from such nanocrystals is no longer comprised of sharp Bragg peaks and broad diffuse background as in

* Corresponding author. Tel.: +1-217-333-682; fax: +1-217-244-2278.
E-mail address: vartaniants@mrl.uiuc.edu (I.A. Vartanyants).
[1] On leave from: Institute of Crystallography RAS, Leninsky Pr. 59, 117333 Moscow, Russia.

0030-4018/03/$ - see front matter
doi:10.1016/S0030-4018(03)01558-X

conventional incoherent scattering but have a complicated intensity distribution centered at each reciprocal-lattice point.

It was shown in the same papers the possibility to invert this continuous diffraction pattern into a real space image. This new type of X-ray microscope may have certain advantages compared with commonly used techniques. In principle, it does not need lenses; its resolution depends on the available coherent flux from the synchrotron source (at the moment a resolution better than 0.1 μm can be achieved) and 3D image of the sample can be obtained conveniently from several adjacent scans of reciprocal space, without need of the 180° rotation of the sample as in tomography [17]. What is most important, due to the high penetration of X-rays, this new X-ray microscope can image the inner parts of the crystal (with all possible inhomogeneities and holes) and additionally with the potential of imaging the strain field inside the crystal [18].

In the first reconstructed images we have seen some additional regions of high intensity that cannot be associated with the nanocrystal structure. Computer simulations assuming partial coherence rather than pure coherence of the incoming beam have shown [19] that additional features observed on the images can be attributed to this partial coherence of the incoming beam. In most previous studies it was assumed that the partial coherence of the incoming beam is associated mainly with a finite size of the source. The same approach was used in our model calculations. However, simple estimations show that for the parameters of the hard X-ray beamline where CXD experiments were performed (APS storage ring) the finite size of the source is not the only origin of the coherence loss. Optical elements present in the beamline can contribute significantly to the possible degradation of coherence of the beam. In addition, the transverse coherence of the beam can change non-uniformly and can contain sharp features on the more uniform background. From this preliminary analysis it has become clear that more detailed analysis of the coherency properties of the beam passing different optical elements is necessary.

It was appreciated from the beginning that partial coherence of the incoming beam can change the apparent scattered intensity distribution from a sample. A comprehensive theoretical study of partial coherence effects on the observed intensity distribution in the far-field as well as in the near-field X-ray scattering was made by Sinha et al. [20]. In a recent paper [21] partial coherence effects on the topography measurements were analyzed. There were even proposals [22] to manipulate with coherency properties of the beam in order to obtain a diffraction pattern from just one protein molecule in a crystal. These different applications of X-ray coherent scattering motivate further theoretical and experimental attempts to understand the coherency properties of the beam on third generation storage rings.

During last decade several attempts were made to measure the coherency properties of the X-ray beams. It is not a trivial problem for X-ray wavelengths of the order of angstrom to measure coherence with a two-slit Young type experiment that is routinely used for the visible light [23]. However, in the soft X-ray region, an interferometric Young type measurement of the spatial coherency properties of the beam was performed [24–26]. To measure spatial coherence in the hard X-ray region different approaches were proposed: to use dynamical diffraction effects to measure the visibility of *Pendellösung* fringes [27], to measure interference pattern from double reflecting mirrors in a kind of two-slit Young experiment [28], to use gratings as a phase object to measure coherence utilizing Talbot effect [29], to make high precision measurements of intensity distribution on well-defined objects as slits in the far-field [30] and more recently slits and fibers in the near-field [31]. Quite different approach of the characterization of transverse coherence by intensity interferometry technique was proposed in [32]. First two-slit Young experiment to measure spatial coherence of the synchrotron beam in hard X-ray energy range was reported only recently [33] (a specially prepared phase mask was used to measure the coherence at APS storage ring [34]). It is important to note here that coherency properties can change essentially from one beamline to another and even on the same beamline they depend on the optics present in experiment.

When the first phase contrast images with coherent X-rays were obtained, it became clear that the quality of the optic elements present in the

beamline can be important for this imaging technique. The height profile of the mirror [35] and the inhomogeneities of the Be window [36] illuminated by coherent beam introduce additional distortion of the wavefront and can produce unavoidable artifact images in the form of speckle pattern and as a result can distort the image of the object. What is more important and was not investigated in detail up to now is that all the optics in the beamline can change the coherency properties of the beam. So it will be desirable to have some method to calculate or at least to estimate effects introduced by an optical element on the coherency properties of the X-ray beam. This is the main goal of this paper.

In visible light optics it is well established that coherency properties of the beam can be described by the so-called mutual coherence function (MCF) that measure correlation between two beams separated in space and time [23,37,38]. The propagation of this MCF in the free space is governed by two wave equations similar to the wave propagation equation obtained directly from Maxwell equations. This general approach can be in principle applied to propagation of any electromagnetic radiation including hard X-rays. The theoretical description is simplified if "quasi-monochromatic" conditions are fulfilled which means that the path length difference between the two beams is less than the longitudinal coherence length. The statistical properties of the beam in the plane across its propagation direction can then be well described by the mutual intensity function (MIF) that gives correlations of two field amplitudes at different points in this plane and the same time. The general propagation laws of this MIF in free space are obtained directly from the corresponding equations for MCF. These main definitions and equations are briefly summarized in Section 2.

In this paper we will be interested in applying this general theory of propagation of the MIF to the special case of propagation of the hard X-rays starting from a conventional "insertion device" (wiggler or undulator) on a third generation X-ray storage ring. It is well known that such source can be well described as an incoherent source of X-ray radiation because each electron is an independent radiator. Typical beamlines at high energy synchrotron radiation sources are built from components which contain optical elements. These are either intended to adapt the qualities of the beam to the needs of the experiment or can do so inadvertently. Important categories of components would be slits, mirrors, monochromators, lenses, and windows. Each of these elements can change in a different way the coherency properties of the beam. We will consider an idealized beamline configuration with only one optic element on the way from the source to the sample. The radiation incoming on this element can be of any state of coherence. Then by applying the general propagation law for the MIF, the coherency properties of the beam at the sample position will be calculated (Section 3). If the detailed structure (slit size, microstructure of the window or height function of the mirror) of the element is known this general approach gives, in principle, the possibility to calculate the MIF and consequently the coherency properties of the beam at the sample position. However, exact knowledge of the optical elements microstructure is often limited. This makes it difficult to predict the coherency properties of the beam at the sample position and different approaches have to be applied.

The following situation is often realized on the beamline: because of the divergence of the beam, the illuminated area on an optical element is much bigger than the coherence length of the incoming radiation. That is especially true for the last element that is usually an exit Be window. The incoming beam is rescattered and refracted due to all inhomogeneities present in the window that cause an unpredictable change of an optical pathlength of X-rays transmitted through that window. In this situation an optical element can be modeled as a random object and its structure can be characterized by statistical parameters such as roughness of the surface and correlation length of the height–height fluctuations. It will be shown (Section 4) that in this case MIF will split into two parts. The first one will describe the propagation of radiation from the source to the sample without rescattering on the optics and will preserve high coherence. The second one takes into consideration the effects of rescattering on the optics and has reduced coherence lengths. The detailed calculation of this

additional contribution is given in Section 5. The short coherence lengths can be explained to a first approximation in the far-field limit by a large effective source size on the window due to divergence of X-ray beam. However, as was discussed in detail in [20], the far-field conditions are easily violated in the case of hard X-rays. It will be shown in the same section, that for the typical parameters of the CXD beamline, the 'sharp' contribution to MIF has to be calculated in the near-field rather then far-field limit.

In the last section such a two-component MIF, calculated for elements with various statistical properties, will be applied to calculate the intensity distribution from a small crystalline particle in a CXD experiment. This intensity distribution is similar to one observed in experiment [16]. Then applying reconstruction procedure discussed in [19] this intensity distribution will be used to obtain the real image of the particle. Additional features that can appear in the image of a nanoparticle due to a reduced coherence of the incoming beam will be discussed.

2. Laws of propagation of the mutual coherence function. Basic equations

The central concept in the theory of partial coherency is the so-called mutual coherence function (MCF) $\Gamma(P_1,P_2;\tau)$ that defines the correlations between two complex scalar[2] values of the electric field at different points P_1 and P_2 and different times. It is defined as

$$\Gamma(P_1,P_2;\tau)=\langle E(P_1,t+\tau)E^*(P_2,t)\rangle_T, \tag{1}$$

where $E(P_1,t+\tau)$ and $E(P_2,t)$ are the field values at the points P_1 and P_2 and brackets $\langle\cdots\rangle_T$ mean an averaging over times T much longer than the fluctuation time of the X-ray field. It is also assumed that the radiation is ergodic and stationary. According to the laws of propagation of partially coherent narrowband radiation ($\Delta\omega\ll\omega$) defined by the Huygens–Fresnel principle [37,38], the MCF propagates from the surface Σ_1 to the surface Σ_2, as shown in Fig. 1, according to

$$\Gamma(Q_1,Q_2;\tau)=\int_{\Sigma_1}\int_{\Sigma_1}\Gamma\left(P_1,P_2;\tau+\frac{R_2-R_1}{c}\right)\times\frac{\mathrm{d}S_1}{\bar{\lambda}R_1}\frac{\mathrm{d}S_2}{\bar{\lambda}R_2}. \tag{2}$$

Here, R_1 and R_2 are the distances between the points P_1 and P_2 on the surface Σ_1 and the points Q_1 and Q_2 on the surface Σ_2, $\bar{\lambda}$ is an average wavelength and c is the speed of light. It is assumed in this expression for the narrow divergent X-ray field that the obliquity factor $\chi(\theta)\approx 1$.

The experiment is defined as "quasi-monochromatic" when it satisfies the condition that the maximum pathlength difference is much smaller than the longitudinal coherence length $R_2-R_1\ll l_{\mathrm{coh}}=\tau_{\mathrm{coh}}c$. Then, according to Goodman [37], the MCF can be written as

$$\Gamma(Q_1,Q_2;\tau)=J(Q_1,Q_2)\,\mathrm{e}^{-\mathrm{i}\varpi\tau}, \tag{3}$$

where

$$J(Q_1,Q_2)=\Gamma(Q_1,Q_2;0)=\langle E(Q_1,t)E^*(Q_2,t)\rangle_T \tag{4}$$

is called the mutual intensity function (MIF) and ϖ is the mean frequency. The MIF specifies the correlations of the fields at different points and the same time. The propagation law for the MIF follows from (2):

$$J(Q_1,Q_2)=\frac{1}{(\bar{\lambda}R)^2}\int_{\Sigma_1}\int_{\Sigma_1}J(P_1,P_2)\,\mathrm{e}^{-\mathrm{i}\bar{k}(R_2-R_1)}\,\mathrm{d}S_1\,\mathrm{d}S_2, \tag{5}$$

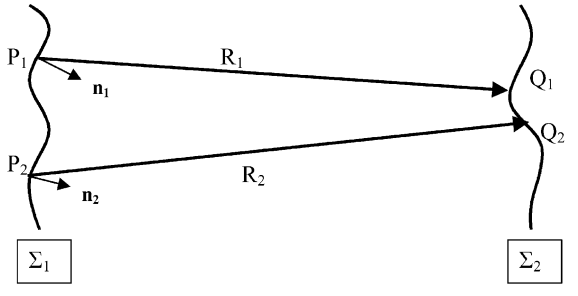

Fig. 1. Propagation of mutual coherence function from surface Σ_1 to surface Σ_2. Vectors $\mathbf{n}_1$ and $\mathbf{n}_2$ are the normal vectors to the surface Σ_1 at points P_1 and P_2.

[2] In the following, for simplicity, we will consider only one polarization of the X-ray field.

where $\overline{k} = 2\pi/\overline{\lambda}$. Here, it has been assumed that, for large distances between the surfaces Σ_1 and Σ_2, the approximation $1/R_1 \approx 1/R_2 \approx 1/R$ is valid. It is usual to normalize the MIF as

$$\mu(Q_1, Q_2) = \frac{J(Q_1, Q_2)}{\sqrt{J(Q_1, Q_1)J(Q_2, Q_2)}}, \tag{6}$$

which is known as complex coherence factor (CCF).

The intensity distribution is obtained directly from (5) by letting $Q_2 \to Q_1$ to give the expression

$$I(Q_1) = J(Q_1, Q_1). \tag{7}$$

3. Propagation of the mutual intensity function through the optical element

We will consider now an idealized situation of the beamline when on the way from the synchrotron source to the sample the X-ray beam passes through *one* optical element (Fig. 2). It can be pair of slits, lens, Be window or a mirror. In the most general way these elements can be characterized by their complex valued amplitude transmittance function $T(\mathbf{u})$. The actual form of the transmittance function may differ from one element to another and will be defined more explicitly below.

We will also assume a "conventional" source of synchrotron radiation (bending magnet, wiggler or undulator) which can be considered to be a planar incoherent source at distance L_1 from the element. The sample is at a distance L_2 behind it (Fig. 2). The source, optical element, and the sample will be described in their "local" 2D coordinate frames perpendicular to the direction of the beam propagation by its coordinates $\mathbf{s}, \mathbf{u}$, and $\mathbf{r}$, respectively. Below, we will tacitly assume that a monochromator is also present in the beamline to provide narrow bandwidth of the X-ray beam and hence provide with high degree of longitudinal coherence length. It will be also considered that the incoming radiation on the element can be partially coherent.

The amplitude of the transmitted beam $A_t(\mathbf{u}, t)$ can be written in terms of the amplitude $A_{in}(\mathbf{u}, t)$ of the incoming beam as

$$A_t(\mathbf{u}, t) = T(\mathbf{u})A_{in}(\mathbf{u}, t - \tau_0), \tag{8}$$

where $T(\mathbf{u})$ is an amplitude transmittance function and τ_0 is an average time delay associated with the structure of the element. In further calculations it will be assumed that the amplitude transmittance function $T(\mathbf{u})$ is independent of wavelength within the narrow bandwidth of the incident radiation. The MIF transmitted through the structure can be easily obtained from (4), (8) (see, for e.g., textbook [37])

$$J_t(\mathbf{u}_1, \mathbf{u}_2) = T(\mathbf{u}_1)T^*(\mathbf{u}_2)J_{in}(\mathbf{u}_1, \mathbf{u}_2). \tag{9}$$

The MIF propagating from such an element to the sample at distance L_2 (Fig. 2) can be obtained according to the general law of propagation of MIF (5)

$$J(\mathbf{r}_1, \mathbf{r}_2) = \frac{1}{(\overline{\lambda}L_2)^2}\int_\Sigma\int_\Sigma T(\mathbf{u}_1)T^*(\mathbf{u}_2)J_{in}(\mathbf{u}_1, \mathbf{u}_2) \times e^{-i\overline{k}(R_2 - R_1)}\, d\mathbf{u}_1\, d\mathbf{u}_2. \tag{10}$$

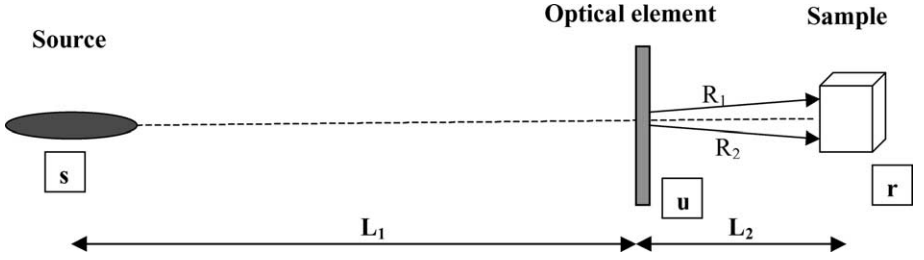

Fig. 2. Beamline with one optical element on the way of propagation of X-rays from the synchrotron source to the sample. The source, element, and the sample are described in their "local" 2D coordinate frames perpendicular to the direction of the beam propagation by their coordinates **s**, **u**, and **r**, respectively.

In the paraxial approximation, when the distance from the element to the sample is much bigger than the effective size of intensity distribution on the element and the size of the sample,

$$R_2 - R_1 \approx 1/2L_2[(\mathbf{r}_2 - \mathbf{u}_2)^2 - (\mathbf{r}_1 - \mathbf{u}_1)^2]$$

and expression for the MIF (10) can be written in the following form:

$$J(\mathbf{r}_1, \mathbf{r}_2) = \int\int T(\mathbf{u}_1) T^*(\mathbf{u}_2) J_{\text{in}}(\mathbf{u}_1, \mathbf{u}_2) P_{L_2}(\mathbf{r}_1 - \mathbf{u}_1) \times P^*_{L_2}(\mathbf{r}_2 - \mathbf{u}_2)\, d\mathbf{u}_1\, d\mathbf{u}_2, \quad (11)$$

where the Green's function (or propagator) $P_{L_2}(\mathbf{r} - \mathbf{u})$ is introduced. It describes the propagation of radiation in free space and is defined as

$$P_{L_2}(\mathbf{r} - \mathbf{u}) = \frac{1}{i\overline{\lambda} L_2} \exp\left[i \frac{\overline{k}}{2L_2} (\mathbf{r} - \mathbf{u})^2\right]. \quad (12)$$

The intensity distribution at the sample position is obtained according to (7) from Eq. (11) by putting $\mathbf{r}_1 = \mathbf{r}_2 = \mathbf{r}$ giving

$$I(\mathbf{r}) = \int\int T(\mathbf{u}_1) T^*(\mathbf{u}_2) J_{\text{in}}(\mathbf{u}_1, \mathbf{u}_2) P_{L_2}(\mathbf{r} - \mathbf{u}_1) \times P^*_{L_2}(\mathbf{r} - \mathbf{u}_2)\, d\mathbf{u}_1\, d\mathbf{u}_2. \quad (13)$$

Expressions (11) and (13) are quite general (their detailed discussion can be found in the textbooks of Goodman [37] and Mandel and Wolf [38]) and relate the coherency properties of the beam incident on the optical element and the coherency properties and intensity distribution reaching the sample. In some sense this element can be regarded as a secondary source defining the coherency properties of the beam on the sample position with MIF $J(\mathbf{r}_1, \mathbf{r}_2)$. Of course different elements modify the coherency properties of the beam in different ways through their specific transmittance function $T(\mathbf{u})$. Below we will analyze in more detail the special case of Be windows or mirrors considered as optical elements on the way from the source to the sample.

A window will be considered as a *thin* object in the sense that X-rays incoming at point $\mathbf{u}$ exit the window essentially at the same transverse coordinate (small refraction effects are neglected). We will also assume that the aperture of the window is essentially bigger than the intensity distribution of the incoming beam. Such element can be characterized by a complex transmittance function

$$T(\mathbf{u}) = B(\mathbf{u})\, e^{i\Phi(\mathbf{u})}, \quad (14)$$

where the amplitude $B(\mathbf{u})$ is responsible for attenuation (absorption) and the phase shift $\Phi(\mathbf{u}) = \overline{\omega}\delta\tau$ is determined by the time delay $\delta\tau$ introduced at point $\mathbf{u}$ by the element. For X-rays propagating through a window characterized by its thickness function $d(\mathbf{u})$ and refractive index $n \simeq 1 - \delta + i\beta$, where δ is the refractive index decrement and β is the absorption index, this time delay introduced at point $\mathbf{u}$ is equal to $\delta\tau = -\delta d(\mathbf{u})/c$. If absorption effects are taken into account, then following Goodman [37], it easy to show that the amplitude $B_{\text{W}}(\mathbf{u})$ and the phase shift $\Phi_{\text{W}}(\mathbf{u})$ at point $\mathbf{u}$ on the window are equal to

$$B_{\text{W}}(\mathbf{u}) = \exp[-\overline{k}\beta d(\mathbf{u})], \quad \Phi_{\text{W}}(\mathbf{u}) = -\overline{k}\delta d(\mathbf{u}), \quad (15)$$

where β and δ can be also position-dependent.

Hypothetically two different types of optics can be considered: purely absorbing (with the phase shift $\Phi(\mathbf{u}) = 0$) and purely refractive (phase objects, with the amplitude function $B(\mathbf{u}) = 1$). In the case of hard X-rays propagating through a Be window, the transmittance function is well approximated by a pure phase function.

Reflecting mirrors are often used on the beamlines as optical elements. Strictly speaking we cannot introduce amplitude transmittance function for the mirrors as it was defined in (8) due to the inversion property (for ideally flat mirror $A_{\text{t}}(-\mathbf{u}) = A_{\text{in}}(\mathbf{u})$). However, it is well known [20,39] that in the case of reflecting rough surface in the first Born approximation the influence of the surface on the incoming amplitude can be associated with the phase factor

$$\Phi_M(\mathbf{u}) = q_z h(\mathbf{u}). \quad (16)$$

Here, q_z is the scattering vector perpendicular to the surface and $h(\mathbf{u})$ is the height function of the surface converted to the coordinate system $\mathbf{u}$ across the beam at the position of the sample. Due to the grazing incident angle conditions, the illuminated area is substantially elongated along the

beam direction. Therefore, coordinate system along the mirror surface itself can be defined as $(u'_x, u'_y = u_x, u_y/\sin\theta)$, where 2θ is the scattering angle. For an ideally flat surface $\Phi_M(\mathbf{u}) = \text{const.}$ and does not change the wave front of the incoming amplitude. However, roughness of the surface will change the phase of the scattered amplitude. So, with some restrictions, a mirror also can be described as a pure phase object by its transmittance function (14) with amplitude $B_M(\mathbf{u}) = 1$ and phase $\Phi_M(\mathbf{u})$ (16).

It is useful to examine several limiting cases of the general expression (11) relating coherency properties of the beam on the sample position with its properties before passing an optical element. Equation (11) was obtained in the paraxial approximation for big distances L_2 between an optical element and the sample. However it gives the correct result even for very small distances. Indeed for $L_2 \to 0$ we have $P_{L_2}(\mathbf{r}-\mathbf{u}) \to \delta(\mathbf{r}-\mathbf{u})$. Substituting this expression in (11) and performing integrations we obtain that mutual intensity function just after an optical element $J(\mathbf{r}_1, \mathbf{r}_2) = T(\mathbf{r}_1)T^*(\mathbf{r}_2)J_{\text{in}}(\mathbf{r}_1, \mathbf{r}_2)$ that is exactly the same as defined in (9).

Now we will consider two limits of coherent and incoherent illumination of the optical element described by the transmittance function $T(\mathbf{u})$ (14). The CCF $\mu_{\text{in}}(\mathbf{u}_1, \mathbf{u}_2)$ defined in (6) being a complex function can be written as $\mu_{\text{in}}(\mathbf{u}_1, \mathbf{u}_2) = |\mu_{\text{in}}(\mathbf{u}_1, \mathbf{u}_2)| \exp[\mathrm{i}\alpha(\mathbf{u}_1) - \mathrm{i}\alpha(\mathbf{u}_2)]$, where $\alpha(\mathbf{u}_1)$ and $\alpha(\mathbf{u}_2)$ are the phases corresponding to points $\mathbf{u}_1$ and $\mathbf{u}_2$ on the optical element. In the *coherent* limit [37,38], $|\mu_{\text{in}}(\mathbf{u}_1, \mathbf{u}_2)| = 1$ which gives for the MIF of the incoming beam $J_{\text{in}}(\mathbf{u}_1, \mathbf{u}_2) = \sqrt{I_{\text{in}}(\mathbf{u}_1)}\sqrt{I_{\text{in}}(\mathbf{u}_2)} \exp[\mathrm{i}\alpha(\mathbf{u}_1) - \mathrm{i}\alpha(\mathbf{u}_2)]$. In the case of the infinitely far source the phases $\alpha(\mathbf{u}_1) = \alpha(\mathbf{u}_2) = \text{const.}$ and can be taken equal to zero. Substituting this expression in Eqs. (11) and (13) gives for the MIF

$$J_{\text{coher}}(\mathbf{r}_1, \mathbf{r}_2) = A(\mathbf{r}_1)A^*(\mathbf{r}_2) \tag{17}$$

and for the intensity distribution

$$I_{\text{coher}}(\mathbf{r}) = |A(\mathbf{r})|^2, \tag{18}$$

where

$$A(\mathbf{r}) = \int T(\mathbf{u})\sqrt{I_{\text{in}}(\mathbf{u})}\,\mathrm{e}^{\mathrm{i}\alpha(\mathbf{u})}P_{L_2}(\mathbf{r}-\mathbf{u})\,\mathrm{d}\mathbf{u}. \tag{19}$$

This is the general expression for the intensity and amplitude of the coherently scattered radiation that takes into account the intensity distribution of the incoming beam and is valid both in the near- and far-field limits. In the case of the non-uniform element described by the transmittance function $T(\mathbf{u})$ (14) expressions (18) and (19) will result in high contrast background speckle patterns on the CCD detector after diffraction from the sample. This effect was observed experimentally for hard X-rays coherently illuminating mirrors [35] and Be windows [36]. Of course this speckle pattern can be significantly reduced by using a uniform window (for example specially polished) with constant amplitude B_{W} and phase shift Φ_{W} across the beam. However, this represents a difficult technical problem for X-ray wavelengths [40].

In the *incoherent* limit of the incoming beam the CCF $\mu_{\text{in}}(\mathbf{u}_1, \mathbf{u}_2)$ can be taken to be a delta function [37,38] $\mu_{\text{in}}(\mathbf{u}_1, \mathbf{u}_2) = \kappa\delta(\mathbf{u}_2 - \mathbf{u}_1)$, where κ is the numerical constant with the dimension of the length squared. In this limit, the MIF of the incoming beam reduces to $J_{\text{in}}(\mathbf{u}_1, \mathbf{u}_2) = \kappa I_{\text{in}}(\mathbf{u}_1) \times \delta(\Delta\mathbf{u})$, where $I_{\text{in}}(\mathbf{u}_1)$ is the intensity distribution of the incoming beam. Substituting this MIF in Eq. (11) we obtain for the MIF at the sample position

$$\begin{aligned} J_{\text{incoher}}(\mathbf{r}_1, \mathbf{r}_2) &= \kappa \int |T(\mathbf{u})|^2 I_{\text{in}}(\mathbf{u}) P_{L_2}(\mathbf{r}_1 - \mathbf{u}) \\ &\quad \times P^*_{L_2}(\mathbf{r}_2 - \mathbf{u})\,\mathrm{d}\mathbf{u} \\ &= \frac{\kappa\,\mathrm{e}^{-\mathrm{i}\psi}}{(\overline{\lambda}L_2)^2} \int |T(\mathbf{u})|^2 I_{\text{in}}(\mathbf{u}) \\ &\quad \times \exp\left[\mathrm{i}\frac{\overline{k}}{L_2}(\mathbf{r}_2 - \mathbf{r}_1)\mathbf{u}\right]\mathrm{d}\mathbf{u}, \end{aligned} \tag{20}$$

where $\psi = (\overline{k}/2L_2)(\mathbf{r}_2^2 - \mathbf{r}_1^2)$ and the explicit form of the propagator function $P_{L_2}(\mathbf{r}-\mathbf{u})$ (12) was used. This expression is in fact the generalization of the well-known van Cittert–Zernike theorem [37,38] for incoherent illumination of an optical element. It is interesting to note here that in the case of pure phase object ($B_{\text{W}}(\mathbf{u}) = 1$) the coherency properties of the beam passing this optical element will depend *only* on the intensity distribution of the incoming beam $I_{\text{in}}(\mathbf{u})$ and will not depend on the phase shift $\Phi_{\text{W}}(\mathbf{u})$, because the

phase distribution in the incoming beams is already spatially random.

Below we will be interested in the situation in between these two limiting cases when the incoming radiation is *partially* coherent.

4. Propagation of the mutual intensity function through a random optical element

For the perfect Be window the partial coherence of the beam incoming on the sample can be attributed entirely to the final size of the incoherent source. The wavefront of the beam passing such ideal optical element will not be affected and will propagate further to the sample position. However, such ideal conditions can be rarely met in practice. It is well known from the previous experiments [36] that Be windows due to technological problems are highly nonuniform in its internal structure and thickness. The average size of the particles in the window can be about 1 μm [41] and give rise to rescattering and diffraction of the incoming beam. It is clear that the detailed structure of the optical imperfections in the window is unknown a priori. As a consequence we will treat the optical distortions on the way of the beam as a random process and we will see how this may affect coherency properties of the beam.

We will show in this section that even if the detailed structure of the transmittance function of an optical element is not known but it rather can be characterized by its averaged statistical properties still the MIF passing such element can be calculated in a straightforward way. We will show that this is the common situation for a beamline optics and that in this case the MIF (11) splits into two components. The first component can be considered "unscattered", propagating through the optics without distortions. The second part represents the scattering by inhomogeneities of the window or roughness of the mirror.

One more important consideration for the legitimacy of the statistical approach is that the transverse coherence length ξ_{in} of the beam incoming on the window must be much smaller than the effective size of the intensity distribution σ_{eff} of the beam: $\xi_{\text{in}} \ll \sigma_{\text{eff}}$. In this limit the incoming radiation consists of a large number of coherent volumes that propagate through the optics and do not interfere with each other. This means that intensities rather then amplitudes corresponding to different coherent volumes have to be summed up. We will also assume that the transverse coherence length of the incoming radiation is macroscopic and is bigger than (or of the order of) the correlation length τ of the spatial fluctuations in the element: $\xi_{\text{in}} \gtrsim \tau$. If τ were bigger than ξ_{in}, then the transverse coherence length would simply "cut off" the spatial fluctuations.

Considering Be window as a random optical element we will describe it by transmittance function $T(\mathbf{u})$ (14) that will now be treated as a function of randomly changing amplitude $B(\mathbf{u})$ and (or) phase $\Phi(\mathbf{u})$. We can consider now the propagation through such an optical element to be a random process as well. Now statistical properties of the beam passing such an optical element can be obtained by averaging over some random variable (amplitude or phase) in the expression for the MIF (11). Performing this kind of averaging we obtain [42]

$$\overline{J}(\mathbf{r}_1,\mathbf{r}_2) = \int\int \Gamma(\mathbf{u}_1,\mathbf{u}_2) J_{\text{in}}(\mathbf{u}_1,\mathbf{u}_2) P_{L_2}(\mathbf{r}_1-\mathbf{u}_1) \times P^*_{L_2}(\mathbf{r}_2-\mathbf{u}_2)\,\mathrm{d}\mathbf{u}_1\,\mathrm{d}\mathbf{u}_2, \tag{21}$$

where

$$\Gamma(\mathbf{u}_1,\mathbf{u}_2) = \overline{T(\mathbf{u}_1)T^*(\mathbf{u}_2)} \tag{22}$$

is the spatial autocorrelation of the amplitude transmittance function. The notation $\overline{TT^*}$ means the averaging according to the following rules: if $z(x)$ is a complex random process then $\overline{z(x_1)z^*(x_2)} = \int\int z_1 z_2^* p_2(y_2,x_2;y_1,x_1)\,\mathrm{d}^2z_1\,\mathrm{d}^2z_2$, where $p_2(z_2,x_2;z_1,x_1)$ is a joint probability density [38]. We want to note here that for the stationary and ergodic process this averaging is equivalent to a spatial averaging whereas $\langle\rangle_T$ implies time averaging of the field amplitudes in (1).

According to Eq. (21) the effect on the coherency properties of the beam passing such random optic element is contained in the autocorrelation function $\Gamma(\mathbf{u}_1,\mathbf{u}_2)$ (22) which characterizes it. Below, we will calculate this autocorrelation function for the special cases of random phase and random absorbing optical element.

For the *random phase* object, the phase $\Phi(\mathbf{u})$ in the transmittance function (14) can be regarded as a random phase shift introduced at point $\mathbf{u}$. For such object the phase of the transmitted X-ray beam can change from point to point in the random way but we neglect absorption processes in the window. We believe that for high energy X-rays passing low Z material such as Be window this is the most appropriate model. We will now assume that this random phase can be modeled as zero-mean $\overline{\Phi(\mathbf{u}_1)} = \overline{\Phi(\mathbf{u}_2)} = 0$ Gaussian random process. Since both $\Phi(\mathbf{u}_1)$ and $\Phi(\mathbf{u}_2)$ are Gaussian, so is the phase difference $\Delta\Phi(\mathbf{u}_1,\mathbf{u}_2) = \Phi(\mathbf{u}_1) - \Phi(\mathbf{u}_2)$. The autocorrelation function for such Gaussian random process can be easily calculated using some results of the theory of probability of the random processes [42],

$$\Gamma(\mathbf{u}_1,\mathbf{u}_2) = \overline{\exp[\mathrm{i}\Delta\Phi(\mathbf{u}_1,\mathbf{u}_2)]} = \exp\left[-\frac{\overline{[\Delta\Phi(\mathbf{u}_1,\mathbf{u}_2)]^2}}{2}\right]. \tag{23}$$

Here, $\overline{[\Delta\Phi(\mathbf{u}_1,\mathbf{u}_2)]^2} = \overline{[\Phi(\mathbf{u}_1) - \Phi(\mathbf{u}_2)]^2}$ is the so-called structure function of the random process $\Phi(\mathbf{u})$. For a wide-sense stationary random process this structure function $\overline{[\Delta\Phi(\Delta\mathbf{u})]^2} = 2\overline{\Phi^2(0)} - 2\overline{\Phi(\mathbf{u})\Phi(\mathbf{u}+\Delta\mathbf{u})}$ and depends only on the coordinate difference $\Delta\mathbf{u} = \mathbf{u}_2 - \mathbf{u}_1$. Substituting this result into (23), we get for the autocorrelation function (22)

$$\Gamma(\Delta\mathbf{u}) = \exp\left\{-\sigma_\Phi^2[1-\gamma_\Phi(\Delta\mathbf{u})]\right\}, \tag{24}$$

where $\sigma_\Phi^2 = \overline{\Phi^2(0)}$ is the variance and $\gamma_\Phi(\Delta\mathbf{u}) = \overline{\Phi(\mathbf{u})\Phi(\mathbf{u}+\Delta\mathbf{u})}/\sigma_\Phi^2$ is the normalized phase autocorrelation function which has the general property of decaying from unity at $\Delta\mathbf{u} = 0$ to zero when $\Delta\mathbf{u} \to \infty$. Expression (24) can be split into a sum of two terms

$$\Gamma(\Delta\mathbf{u}) = \mathrm{e}^{-\sigma_\Phi^2} + \mathrm{e}^{-\sigma_\Phi^2}\left[\mathrm{e}^{\sigma_\Phi^2\gamma_\Phi(\Delta\mathbf{u})} - 1\right] = E^2 + E^2 g_\Phi(\Delta\mathbf{u}), \tag{25}$$

where

$$E^2 = \exp(-\sigma_\Phi^2), \quad g_\Phi(\Delta\mathbf{u}) = \left[\mathrm{e}^{\sigma_\Phi^2\gamma_\Phi(\Delta\mathbf{u})} - 1\right]. \tag{26}$$

In the limit of small variance $\sigma_\Phi^2 \ll 1$, we have from (26) an approximate expression

$$g_\Phi(\Delta\mathbf{u}) \simeq \sigma_\Phi^2\gamma_\Phi(\Delta\mathbf{u}). \tag{27}$$

The variance σ_Φ^2 in the case of the uniform window is equal to $\sigma_\Phi^2 = \overline{k}^2\delta^2\sigma_d^2$, where $\sigma_d^2 = \overline{d^2(\mathbf{u})}$ is the variance for the thickness fluctuations. For the non-uniform Be window, the variance of the refractive index σ_δ^2 has to be also included giving $\sigma_\Phi^2 = \overline{k}^2(\sigma_\delta^2 + \sigma_d^2)$. The variance for the reflecting mirror is equal to $\sigma_\Phi^2 = q_z^2\sigma_h^2$, where $\sigma_h^2 = \overline{h^2(\mathbf{u})}$ is the variance for the height fluctuations on the surface of the mirror.

The form of the normalized autocorrelation function $\gamma_\Phi(\Delta\mathbf{u})$ depends on the type of fluctuations in the element. It is usual to parametrize it with a finite number of parameters. The simplest model for the autocorrelation function that satisfies its general properties is in the form of exponential function

$$\gamma_\Phi(\Delta\mathbf{u}) = \exp(-|\Delta\mathbf{u}|/\tau), \tag{28}$$

where τ is the lateral correlation length of the fluctuations. For the height–height fluctuations on the surface, a more general form of the autocorrelation function $\gamma_\Phi(\Delta\mathbf{u})$ was proposed by Sinha et al. [39]

$$\gamma_h(\Delta\mathbf{u}) = \exp[-(|\Delta\mathbf{u}|/\tau)^{2\alpha}], \tag{29}$$

where the roughness exponent α is included. This expression gives a power law $\sim (|\Delta\mathbf{u}|/\tau)^{2\alpha}$ appropriate for the short-range correlations. For the roughness parameter $\alpha = 1/2$, this definition of $\gamma_h(\Delta\mathbf{u})$ coincides with the exponential form (28).

For generality the *random absorbing* window can be also considered. In this case it is the amplitude $B(\mathbf{u})$ of the transmittance function (14) that is considered as a random function for the X-rays propagating through the window. At the same time we neglect the change of the phase $\Phi(\mathbf{u})$. According to Goodman [37], in the case of the random absorbing window the autocorrelation function (22) can be also presented as a sum of two terms

$$\Gamma(\Delta\mathbf{u}) = T_0^2 + g_t(\Delta\mathbf{u}), \quad g_t(\Delta\mathbf{u}) = \sigma_t^2\gamma_t(\Delta\mathbf{u}), \tag{30}$$

where T_0 is real and non-negative $0 \leqslant T_0 \leqslant 1$, σ_t^2 is variance and $\gamma_t(\Delta\mathbf{u})$ is the normalized autocorrelation function of the random fluctuations. The same exponential model (28) can be taken for the autocorrelation function $\gamma_t(\Delta\mathbf{u})$.

Now, substituting the expressions obtained for the autocorrelation function $\Gamma(\Delta\mathbf{u})$ for the random phase (25) and random absorbing (30) optical element into the expression for the MIF (21), we obtain

$$\overline{J}(\mathbf{r}_1,\mathbf{r}_2) = C_1 J_{\mathrm{S}}(\mathbf{r}_1,\mathbf{r}_2) + C_2 J_{\mathrm{W}}(\mathbf{r}_1,\mathbf{r}_2), \tag{31}$$

where

$$J_{\mathrm{S}}(\mathbf{r}_1,\mathbf{r}_2) = \int\int J_{\mathrm{in}}(\mathbf{u}_1,\mathbf{u}_2) P_{L_2}(\mathbf{r}_1-\mathbf{u}_1) \times P^*_{L_2}(\mathbf{r}_2-\mathbf{u}_2)\,\mathrm{d}\mathbf{u}_1\,\mathrm{d}\mathbf{u}_2 \tag{32}$$

describes the part of MIF that propagates directly from the source through the window without any distortion and

$$J_{\mathrm{W}}(\mathbf{r}_1,\mathbf{r}_2) = \int\int g(\Delta\mathbf{u}) J_{\mathrm{in}}(\mathbf{u}_1,\mathbf{u}_2) P_{L_2}(\mathbf{r}_1-\mathbf{u}_1) \times P^*_{L_2}(\mathbf{r}_2-\mathbf{u}_2)\,\mathrm{d}\mathbf{u}_1\,\mathrm{d}\mathbf{u}_2 \tag{33}$$

is the part that is changed due to propagation through the random structure of the window or mirror. In Eq. (31), coefficients C_1 and C_2 are equal to $C_1 = C_2 = E^2$ for the random phase element and $C_1 = T_0^2, C_2 = 1$ for the random absorbing window. Function $g(\Delta\mathbf{u})$ is defined in (26) and (30).

It can be shown (see Appendix A for details) that the undistorted part of the MIF $J_{\mathrm{S}}(\mathbf{r}_1,\mathbf{r}_2)$ travelling a distance L_1 from the source followed by a distance L_2 to the sample can be calculated according to the van Cittert–Zernike theorem [23,37,38] as

$$J_{\mathrm{S}}(\mathbf{r}_1,\mathbf{r}_2) = \kappa \frac{\mathrm{e}^{-\mathrm{i}\psi_{\mathrm{S}}}}{[\overline{\lambda}(L_1+L_2)]^2} \int_{\Sigma} I_{\mathrm{S}}(\mathbf{s}) \times \exp\left[\mathrm{i}\frac{\overline{k}}{L_1+L_2}(\mathbf{r}_2-\mathbf{r}_1)\mathbf{s}\right]\mathrm{d}\mathbf{s}, \tag{34}$$

where $\psi_{\mathrm{S}} = \overline{k}/[2(L_1+L_2)](\mathbf{r}_2^2-\mathbf{r}_1^2)$, $I_{\mathrm{S}}(\mathbf{s})$ is the intensity distribution of the incoherent source and integration is performed over the whole area of the incoherent source, Σ.

The intensity distribution for a generic synchrotron radiation source will be taken in the form of a Gaussian function

$$I_{\mathrm{S}}(s_x,s_y) = I_0 \exp\left[-\frac{s_x^2}{2\sigma_x^2} - \frac{s_y^2}{2\sigma_y^2}\right], \tag{35}$$

where σ_x and σ_y are the halfwidths of the intensity distribution in the horizontal (x) and vertical (y) directions. This represents an approximation for the shape of the electron "bunches" within the storage ring.

Typical numbers for a CXD experiment can now be estimated as follows. The distance from the synchrotron source to the sample is $L_1 + L_2 \simeq 60$ m. At an energy $E_\gamma \simeq 8$ keV, the far-field condition $\overline{k}D^2/[2(L_1+L_2)] \ll 1$ is easily satisfied for samples of micron size. In this far-field limit we can neglect the phase prefactor $\exp[\mathrm{i}\psi]$ in Eq. (34) to obtain an extremely simple (Fourier transform) connection between the source intensity distribution and the coherency properties of the beam reaching the sample.

Integration in Eq. (34) with the typical intensity distribution (35) gives for the MIF

$$J_{\mathrm{S}}(\mathbf{r}_2-\mathbf{r}_1) = \kappa \frac{2\pi\sigma_x\sigma_y I_0}{[\overline{\lambda}(L_1+L_2)]^2} \exp\left[-\frac{\Delta x^2}{2\xi_{\mathrm{S}x}^2} - \frac{\Delta y^2}{2\xi_{\mathrm{S}y}^2}\right], \tag{36}$$

where

$$\xi_{\mathrm{S}x,y} = \frac{L_1+L_2}{\overline{k}\sigma_{x,y}} \tag{37}$$

is the transverse coherence length at the sample position given by the size of the incoherent source $\sigma_{x,y}$ and distance from the source to sample L_1+L_2.

Typical numbers for coherence length that might apply in CXD experiments can be estimated for the APS source [44]. The size of the source in horizontal $\sigma_x \simeq 250$ and vertical $\sigma_y \simeq 50$ μm directions gives transverse coherence lengths $\xi_{\mathrm{S}x} \simeq 6$ and $\xi_{\mathrm{S}y} \simeq 30$ μm at 8 keV. If the typical size of the sample (for example a particle of micron size) or the size of the slits before the sample is less then these coherence lengths $D \ll \xi_{\mathrm{S}}$, then experiment is regarded as coherent. However, we will show below that this is a necessary, but not a sufficient, condition to obtain a pure coherent illumination of the sample in the beamline. The second term in the MIF $\overline{J}(\mathbf{r}_1,\mathbf{r}_2)$ can also change the effective coherence lengths that affect the outcome of an experiment.

5. Contribution to the coherency properties of the beam from rescattering from random optical element

In this section we will discuss in detail the second term $J_W(\mathbf{r}_1,\mathbf{r}_2)$ (33) in expression for the total MIF $\overline{J}(\mathbf{r}_1,\mathbf{r}_2)$ (31). According to definition of the CCF (6) the MIF in the incoming beam is $J_{in}(\mathbf{u}_1,\mathbf{u}_2)=\sqrt{I_{in}(\mathbf{u}_1)}\sqrt{I_{in}(\mathbf{u}_2)}\mu_{in}(\mathbf{u}_1,\mathbf{u}_2)$. In the often-used quasi-homogeneous approximation, the CCF of the incoming beam $\mu_{in}(\mathbf{u}_1,\mathbf{u}_2)$ depends only on the difference of the coordinates $\Delta\mathbf{u}=\mathbf{u}_2-\mathbf{u}_1$ and is characterized by its coherence length ξ_{in}. Further it is assumed that the width of the intensity distribution $I_{in}(\mathbf{u})$ in the incoming beam is much bigger than the transverse coherence area A_{coh} (as used in (21)) and that this intensity distribution is a slow varying function on the size of A_{coh}. In this quasi-homogeneous approximation, the MIF of the incoming beam can be written as

$$J_{in}(\mathbf{u}_1,\mathbf{u}_2)=I_{in}(\overline{\mathbf{u}})\mu_{in}(\Delta\mathbf{u}), \tag{38}$$

where $\overline{\mathbf{u}}=(\mathbf{u}_1+\mathbf{u}_2)/2$. Both, the intensity distribution $I_{in}(\overline{\mathbf{u}})$ and CCF $\mu_{in}(\Delta\mathbf{u})$ of the incoming beam, can be assumed to be Gaussian. The intensity distribution is taken with the constant prefactor I_0^{in} and halfwidths $\sigma_{(eff)x,y}$ in the horizontal (x) and vertical (y) directions and CCF

$$\mu_{in}(\Delta\mathbf{u})=\exp\left[-\frac{\Delta u_x^2}{2\xi_{(in)x}^2}-\frac{\Delta u_y^2}{2\xi_{(in)y}^2}\right], \tag{39}$$

where $\xi_{(in)x,y}$ are the typical coherence lengths of the incoming beam. For the beamline set-up shown in Fig. 2 with an incoherent source far away from the optical element this will be an exact result in the far-field limit according to van Cittert–Zernike theorem. In this case coherence lengths will be defined by an expression similar to (37)

$$\xi_{(in)x,y}=\frac{L_1}{\overline{k}\sigma_{x,y}}, \tag{40}$$

where $\sigma_{x,y}$ is the size of the primary source.

Substituting expression (38) in Eq. (33) we get for the MIF at the sample position

$$J_W(\overline{\mathbf{r}},\Delta\mathbf{r})=\frac{e^{-i\psi}}{(\overline{\lambda}L_2)^2}\int\int g(\Delta\mathbf{u})I_{in}(\overline{\mathbf{u}})\mu_{in}(\Delta\mathbf{u})\times\exp\left[-i\frac{\overline{k}}{L_2}(\overline{\mathbf{u}}\Delta\mathbf{u}-\overline{\mathbf{u}}\Delta\mathbf{r}-\overline{\mathbf{r}}\Delta\mathbf{u})\right]d\overline{\mathbf{u}}\,d\Delta\mathbf{u}, \tag{41}$$

where $\psi=(\overline{k}/L_2)(\overline{\mathbf{r}}\Delta\mathbf{r})$, $\overline{\mathbf{r}}=(\mathbf{r}_1+\mathbf{r}_2)/2$ and $\Delta\mathbf{r}=\mathbf{r}_2-\mathbf{r}_1$. In deriving Eq. (41) the explicit form of propagators $P_{L_2}(\mathbf{r}-\mathbf{u})$ (12) and identity $(1/2L_2)[(\mathbf{r}_2-\mathbf{u}_2)^2-(\mathbf{r}_1-\mathbf{u}_1)^2]=(1/L_2)(\overline{\mathbf{r}}\Delta\mathbf{r}+\overline{\mathbf{u}}\Delta\mathbf{u}-\overline{\mathbf{u}}\Delta\mathbf{r}-\overline{\mathbf{r}}\Delta\mathbf{u})$ were used.

The intensity distribution of the beam at the sample position is obtained directly from Eq. (41) by the substitution $\mathbf{r}_1=\mathbf{r}_2=\mathbf{r}$ so that $\Delta\mathbf{r}=0$ and the phase factor $\psi=0$

$$I_W(\overline{\mathbf{r}})=\frac{1}{(\overline{\lambda}L_2)^2}\int\int g(\Delta\mathbf{u})I_{in}(\overline{\mathbf{u}})\mu_{in}(\Delta\mathbf{u})\times\exp\left[-i\frac{\overline{k}}{L_2}(\overline{\mathbf{u}}\Delta\mathbf{u}-\overline{\mathbf{r}}\Delta\mathbf{u})\right]d\overline{\mathbf{u}}\,d\Delta\mathbf{u}. \tag{42}$$

We want to note here that these expressions for the MIF $J_W(\overline{\mathbf{r}},\Delta\mathbf{r})$ and the intensity distribution $I_W(\overline{\mathbf{r}})$ are valid both for the far-field and the near-field approximation so long as quasi-homogeneous illumination (38) is assumed. We will consider separately two limits of these expressions.

Far-field limit. The simplest expressions for the MIF $J_W(\overline{\mathbf{r}},\Delta\mathbf{r})$ and the intensity distribution $I_W(\overline{\mathbf{r}})$ can be obtained when the following condition is valid $(\overline{k}/L_2)\overline{\mathbf{u}}\Delta\mathbf{u}\ll\pi/2$, which defines the far-field limit, so that this phase factor can be neglected in the exponent in (41) and (42). This gives for the distance L_2

$$L_2\gg 2\sigma_{eff}\xi_{in}/\overline{\lambda}, \tag{43}$$

where σ_{eff} is an effective size of the spatial intensity distribution of the beam reaching the optics and ξ_{in} is the transverse coherence length of this beam. If correlation lengths τ of the element are much less than the coherence length of the incoming beam, then in expression (43) ξ_{in} has to be substituted by τ.

In this far-field limit, the MIF (41) factorizes and can be written as a product of two functions

$$J_W^{FF}(\overline{\mathbf{r}},\Delta\mathbf{r})=I_W^{FF}(\overline{\mathbf{r}})\cdot\mu_W^{FF}(\Delta\mathbf{r}), \tag{44}$$

where the intensity distribution at the sample position and the CCF are given by

$$I_{\mathrm{W}}^{\mathrm{FF}}(\bar{\mathbf{r}}) = \frac{\int I_{\mathrm{in}}(\mathbf{u})\,\mathrm{d}\mathbf{u}}{(\bar{\lambda}L_2)^2}\int g(\Delta\mathbf{u})\mu_{\mathrm{in}}(\Delta\mathbf{u}) \times \exp[\mathrm{i}(\bar{k}/L_2)\bar{\mathbf{r}}\Delta\mathbf{u}]\,\mathrm{d}\Delta\mathbf{u}, \tag{45}$$

$$\mu_{\mathrm{W}}^{\mathrm{FF}}(\Delta\mathbf{r}) = \frac{1}{\int I_{\mathrm{in}}(\mathbf{u})\,\mathrm{d}\mathbf{u}}\int I_{\mathrm{in}}(\mathbf{u}) \times \exp[\mathrm{i}(\bar{k}/L_2)\Delta\mathbf{r}\mathbf{u}]\,\mathrm{d}\mathbf{u}. \tag{46}$$

Here, due to far-field conditions (43), the contribution of the phase factor ψ in CCF $\mu_{\mathrm{W}}^{\mathrm{FF}}(\Delta\mathbf{r})$ can be neglected. As it follows from (46) in the far-field limit the coherency properties of the beam on the sample position are determined only by the intensity distribution $I_{\mathrm{in}}(\mathbf{u})$ of the incoming beam on the optical element.

For the Gaussian distribution of the incoming intensity the CCF $\mu_{\mathrm{W}}^{\mathrm{FF}}(\Delta\mathbf{r})$ (46) will also be Gaussian

$$\mu_{\mathrm{W}}^{\mathrm{FF}}(\Delta\mathbf{r}) = \exp\left[-\frac{\Delta x^2}{2\xi_{\mathrm{W}x}^2} - \frac{\Delta y^2}{2\xi_{\mathrm{W}y}^2}\right], \tag{47}$$

where $\xi_{\mathrm{W}x,y}$ is a coherence length determined by the effective size of the source on the optical element

$$\xi_{\mathrm{W}x,y} = \frac{L_2}{\bar{k}\cdot\sigma_{(\mathrm{eff})x,y}}. \tag{48}$$

So, in this far-field limit the coherency properties of the beam scattered from the optics are determined by an effective source size σ_{eff} and distance L_2 from this element. Taking into account that for the last optical element in the beamline usually $L_2 \ll L_1$ and $\sigma_{(\mathrm{eff})} \gg \sigma$, where σ is the size of the synchrotron source we immediately have an estimate $\xi_{\mathrm{W}} \ll \xi_{\mathrm{S}}$, where ξ_{S} (37) is the coherence length produced by the source itself. Since both these inequalities typically represent factors of 10 or more, their combined effect is rather substantial.

For a typical CXD experiment the effective size of the source on the Be window or mirror is determined by the divergence of the beam. The divergence of the beam from a synchrotron source is usually small but finite and is of the order of few μrad. A specific example is the angular distribution of the nth harmonic of an undulator source which has a half-width [45]

$$\sigma' \simeq \frac{1}{\gamma}\sqrt{\frac{1+K^2/2}{2nN_{\mathrm{und}}}}, \tag{49}$$

where γ is the relativistic parameter, K is the deflection parameter (of order unity), and N_{und} is the number of undulator periods. For an undulator at a 7-GeV storage ring with an effective $N_{\mathrm{und}} \approx 50$, the half-width of the angular divergence is expected to be $\sigma' \approx 10$ μrad. The standard "Undulator A" at the APS has a horizontal half-width divergence of $\sigma'_x = 26$ and $\sigma'_y = 14$ μrad in the vertical. This determines the size of the entire beam at the last optical element (usually a Be window) at position $L_1 = 55$ m to be

$$\begin{aligned}\sigma_{(\mathrm{eff})x} &\simeq \sigma_x + \sigma'_x L_1 = 1.7\ \mathrm{mm};\\ \sigma_{(\mathrm{eff})y} &\simeq \sigma_y + \sigma'_y L_1 = 0.8\ \mathrm{mm}.\end{aligned} \tag{50}$$

For this effective source size and distances between the last Be window and the sample that might be typically about $L_2 \simeq 5$ m, we obtain coherence lengths $\xi_{\mathrm{W}x} = 0.07$ and $\xi_{\mathrm{W}y} = 0.15$ μm in the horizontal and the vertical directions. Evidently these coherence lengths are much shorter than coherence lengths produced by the beam propagating directly from the source (37). As we see from this analysis, rescattering in the optics placed in the beam introduces a new, shorter, coherence length at the sample position.

It is important also to analyze the expression for the *intensity distribution* $I_{\mathrm{W}}^{\mathrm{FF}}(\bar{\mathbf{r}})$ (45) in the far-field. Substituting the function $g_{\Phi}(\Delta\mathbf{u})$ (26) gives

$$I_{\mathrm{W}}^{\mathrm{FF}}(\mathbf{q}_{\mathbf{r}}) \propto \int\left[\mathrm{e}^{\sigma_{\Phi}^2\gamma_{\Phi}(\Delta\mathbf{u})} - 1\right]\mu_{\mathrm{in}}(\Delta\mathbf{u}) \times \exp[\mathrm{i}\mathbf{q}_{\mathbf{r}}\Delta\mathbf{u}]\,\mathrm{d}\Delta\mathbf{u}, \tag{51}$$

where $\mathbf{q}_{\mathbf{r}} = (k/L_2)\bar{\mathbf{r}}$. This expression is in fact a generalization of the intensity of the diffuse scattering in the first Born approximation for the partial coherent incoming beam. Really, in the case of scattering from a rough surface in the coherent limit $\mu_{\mathrm{in}}(\Delta\mathbf{u}) = 1$ with variance $\sigma_{\Phi}^2 = q_z^2\sigma_h^2$ and autocorrelation function $\gamma_h(\Delta\mathbf{u})$ (29), Eq. (51) coincides with the well-known expression from [39]. Examination of Eq. (51) shows that unlike the

CCF the intensity distribution in the far-field depends on the imperfections of the optics.

Now, taking the limit of small variance $\sigma_\Phi^2 \ll 1$ in Eq. (51), the exponential form (28) for the autocorrelation function $\gamma_\Phi(\Delta\mathbf{u})$ and assuming Gaussian CCF $\mu_{\rm in}(\Delta\mathbf{u})$ (39), we get for the intensity distribution in the far-field limit

$$I_{\rm W}^{\rm FF}(\mathbf{q}_\mathbf{r}) = I_0^{\rm FF}\cdot\mathscr{I}^{\rm FF}(\mathbf{q}_\mathbf{r}) = \frac{I_0^{\rm FF}}{\xi_{({\rm in})x}\xi_{({\rm in})y}}\int \exp\Big[-|\Delta\mathbf{u}|/\tau - \Delta u_x^2/2\xi_{({\rm in})x}^2 - \Delta u_y^2/2\xi_{({\rm in})y}^2\Big]\exp(i\mathbf{q}_\mathbf{r}\Delta\mathbf{u})\,{\rm d}(\Delta\mathbf{u}), \quad (52)$$

where $I_0^{\rm FF} = 2\pi\sigma_\Phi^2\sigma_{({\rm eff})x}\sigma_{({\rm eff})y}\xi_{({\rm in})x}\xi_{({\rm in})y}I_0^{\rm in}/(\overline{\lambda}L_2)^2$ [46]. If coherence lengths $\xi_{({\rm in})x} = \xi_{({\rm in})y} = \xi_{({\rm in})}$, then integral in (52) can be calculated in circular coordinates giving

$$\mathscr{I}^{\rm FF}(q_r) = \frac{2\pi}{\xi_{({\rm in})}^2}\int_0^\infty \exp\Big[-\rho/\tau - \rho^2/(2\xi_{({\rm in})}^2)\Big]\times J_0(q_r\rho)\rho\,{\rm d}\rho, \quad (53)$$

where $J_0(z)$ is a Bessel function of a zero order and $q_r = |\mathbf{q}_\mathbf{r}|$. As it follows from (52) in the limit $\sigma_\Phi^2 \ll 1$ the intensity $I_{\rm W}^{\rm FF}(\mathbf{q}_\mathbf{r})$ is directly proportional to the variance σ_Φ^2. Consequently this contribution can be made smaller by improving the quality of the optics. It is interesting to note that in the limit of big correlation lengths $\tau \gg \xi_{({\rm in})}$ expressions (52) and (53) give Gaussian distribution of intensity $I_{\rm W}^{\rm FF}(q_r) \propto \exp(-q_r^2\xi_{({\rm in})}^2/2)$. In the opposite limit of big coherence lengths $\xi_{({\rm in})} \gg \tau$ we get for intensity distribution $I_{\rm W}^{\rm FF}(q_r) \propto t^2/(1+q_r^2t^2)^{3/2}$.

The far-field expression for the MIF $J_{\rm W}(\overline{\mathbf{r}},\Delta\mathbf{r})$ (44) is valid only for distances L_2 satisfying condition (43). Simple estimates show that this condition is easily violated in the case of the hard X-rays. A typical CXD experiment might have its last Be window at $L_1 \sim 50$ m. For this configuration the intensity distribution on the window will be about (50) $\sigma_{\rm eff} \sim 1.5$ mm and transverse coherence length of the incoming beam (40) $\xi_{({\rm in})} \sim 10$ μm. This would require $L_2 \gg 2\times 10^2$ m to achieve the far-field limit condition (43) which is difficult to realize in practice. So it is important to understand how this result changes in the near-field limit.

Near-field limit. In the near field limit the phase term $(\overline{k}/L_2)(\overline{\mathbf{u}}\Delta\mathbf{u})$ in the expression for the MIF $J_{\rm W}(\overline{\mathbf{r}},\Delta\mathbf{r})$ (41) has to be taken into account explicitly. In general in this limit, the coherency properties of the beam can be different for different positions in the transverse plane $\mathbf{r}$ at the sample position. However, to simplify the analysis we will calculate the MIF $J_{\rm W}(\overline{\mathbf{r}},\Delta\mathbf{r})$ only for the center of the illuminated region which means that we can put $\overline{\mathbf{r}} = 0$ in (41). For this practically important case the MIF can be written in the following form:

$$J_{\rm W}^{\rm NF}(\Delta\mathbf{r}) = \frac{1}{(\overline{\lambda}L_2)^2}\int {\rm d}(\Delta\mathbf{u})g(\Delta\mathbf{u})\mu_{\rm in}(\Delta\mathbf{u})\times\int {\rm d}\overline{\mathbf{u}}I_{\rm in}(\overline{\mathbf{u}})\,{\rm e}^{-i\mathbf{q}'\overline{\mathbf{u}}}, \quad (54)$$

where $\mathbf{q}' = (k/L_2)(\Delta\mathbf{u}-\Delta\mathbf{r})$. This expression can be calculated further with the same approximations that were used in the far-field limit: the Gaussian distribution of the incoming intensity $I_{\rm in}(\overline{\mathbf{u}})$ with halfwidths $\sigma_{({\rm eff})x} = \sigma_{({\rm eff})y} = \sigma_{({\rm eff})}$ (in this approximation according to definition (48) $\xi_{{\rm W},x} = \xi_{{\rm W},y} = \xi_{\rm W}$), the exponential form (28) for the autocorrelation function $\gamma_\Phi(\Delta\mathbf{u})$ and the Gaussian form (39) for the incoming CCF $\mu_{\rm in}(\Delta\mathbf{u})$. This gives for the MIF $J_{\rm W}^{\rm NF}(\Delta\mathbf{r})$ (54) in the near-field limit

$$J_{\rm W}^{\rm NF}(\Delta\mathbf{r}) = I_0^{\rm NF}\cdot\mu_{\rm W}^{\rm NF}(\Delta\mathbf{r}), \quad (55)$$

where $I_0^{\rm NF} = 2\pi\sigma_\Phi^2\sigma_{({\rm eff})}^2\xi_{\rm W}^2I_0^{\rm in}\mathscr{J}(0)/(\overline{\lambda}L_2)^2$ and

$$\mu_{\rm W}^{\rm NF}(\Delta\mathbf{r}) = \mu_{\rm W}^{\rm FF}(\Delta\mathbf{r})\cdot\mathscr{J}(\Delta\mathbf{r})/\mathscr{J}(0) \quad (56)$$

is the CCF in the near-field. In this expression $\mu_{\rm W}^{\rm FF}(\Delta\mathbf{r})$ is the far-field limit of CCF (47) with the coherence length $\xi_{\rm W}$ (48) and the integral $\mathscr{J}(\Delta\mathbf{r})$ have the following form:

$$\mathscr{J}(\Delta\mathbf{r}) = \frac{1}{\xi_{\rm W}^2}\int \exp\Big[-|\Delta\mathbf{u}|/\tau - \Delta u_x^2/(2\overline{\xi}_x^2) - \Delta u_y^2/(2\overline{\xi}_y^2) + \Delta\mathbf{u}\Delta\mathbf{r}/\xi_{\rm W}^2\Big]\,{\rm d}(\Delta\mathbf{u}), \quad (57)$$

where $\overline{\xi}_{x,y}^2 = \xi_{({\rm in})x,y}^2\xi_{\rm W}^2/(\xi_{({\rm in})x,y}^2+\xi_{\rm W}^2)$. Expression (56) give multiplicative corrections for the far-field result of Eq. (46). It is important to note that unlike the far-field limit results the CCF $\mu_{\rm W}^{\rm NF}(\Delta\mathbf{r})$ in the near-field limit now depends on the statistical properties of the Be window through the correlation length τ. Integral in Eq. (57) can be further calculated if we take into account that for the

typical beamline $\xi_{(\mathrm{in})x,y} \gg \xi_{\mathrm{W}}$ that gives a good approximation $\overline{\xi}_{x,y} \approx \xi_{\mathrm{W}}$. Using circular coordinates, we obtain

$$\mathscr{J}(\Delta r) = \frac{2\pi}{\xi_{\mathrm{W}}^2}\int_0^\infty \exp\left[-\rho/\tau - \rho^2/(2\xi_{\mathrm{W}}^2)\right] \times I_0\left(\rho\Delta r/\xi_{\mathrm{W}}^2\right)\rho\,\mathrm{d}\rho, \quad (58)$$

where $I_0(z)$ is a modified Bessel function of a zero order and $\Delta r = |\Delta\mathbf{r}|$.

The *intensity distribution* in the near-field can be obtained directly from (42). With the same approximations as were made for the calculation of the MIF $J_{\mathrm{W}}^{\mathrm{NF}}(\Delta\mathbf{r})$ (54) and (55), we get

$$I_{\mathrm{W}}^{\mathrm{NF}}(\mathbf{q}_\mathbf{r}) = I_0^{\mathrm{NF}}\cdot\mathscr{I}^{\mathrm{NF}}(\mathbf{q}_\mathbf{r}) = \frac{I_0^{\mathrm{NF}}}{\xi_{\mathrm{W}}^2}\int \exp\left[-|\Delta\mathbf{u}|/\tau - \Delta u_x^2/(2\overline{\xi}_x^2) - \Delta u_y^2/(2\overline{\xi}_y^2)\right] \times \exp(\mathrm{i}\mathbf{q}_\mathbf{r}\Delta\mathbf{u})\,\mathrm{d}(\Delta\mathbf{u}), \quad (59)$$

where $\mathbf{q}_\mathbf{r}$ is defined in (51). It is interesting to note that this near-field intensity distribution has the same form as the far-field expression (53) with the only change of $\overline{\xi}$ to $\xi_{(\mathrm{in})}$ that correspond to the limit $\xi_{\mathrm{W}} \to \infty$ in Eq. (59). Assuming again that $\overline{\xi}_{x,y} \approx \xi_{\mathrm{W}}$ and using circular coordinates we obtain for the integral $\mathscr{I}^{\mathrm{NF}}(\mathbf{q}_\mathbf{r})$ the following expression:

$$\mathscr{I}^{\mathrm{NF}}(q_r) = \frac{2\pi}{\xi_{\mathrm{W}}^2}\int_0^\infty \exp\left[-\rho/\tau - \rho^2/(2\xi_{\mathrm{W}}^2)\right] \times J_0(q_r\rho)\rho\,\mathrm{d}\rho, \quad (60)$$

where $q_r = |\mathbf{q}_\mathbf{r}|$.

Summarizing the results of this section we see that generally speaking, imperfections of the windows and mirrors are the sources of the reduced coherence on the beamline. If the statistical properties (roughness, correlation length, etc.) of an element are known, the magnitude of these coherence lengths can be estimated from the expressions derived in this section. It is important to note that the "decoherence" effect of optics is not a degradation of the inherent source coherence, but instead the creation of an entirely new component to the coherence function with a dramatically reduced coherence length. This is illustrated schematically in Fig. 3. If more than one optical element is present the formalism generalizes in a straightforward way to further components added to MIF.

As an example in Fig. 4 we present the results of a calculation using the formalism described in this section of the complex coherence factor $\mu(\Delta x, \Delta y) = \overline{J}(\Delta x, \Delta y)/\overline{J}(0)$ calculated for the X-ray radiation with wavelength $\overline{\lambda} = 1.5$ Å propagating through a random phase optical element at a distance $L_2 = 6$ m from the sample. This element is located at $L_1 = 56$ m from an incoherent source of size $\sigma_x = 250$ μm in the horizontal direction (left panel in Fig. 4) and $\sigma_y = 50$ μm in the vertical direction (right panel in Fig. 4). An effective source size of the beam on the optical element $\sigma_{(\mathrm{eff})x,y}$ and parameters characterizing the statistical properties of an element (variance σ_ϕ^2 and longitudinal correlation length τ) used in calculations

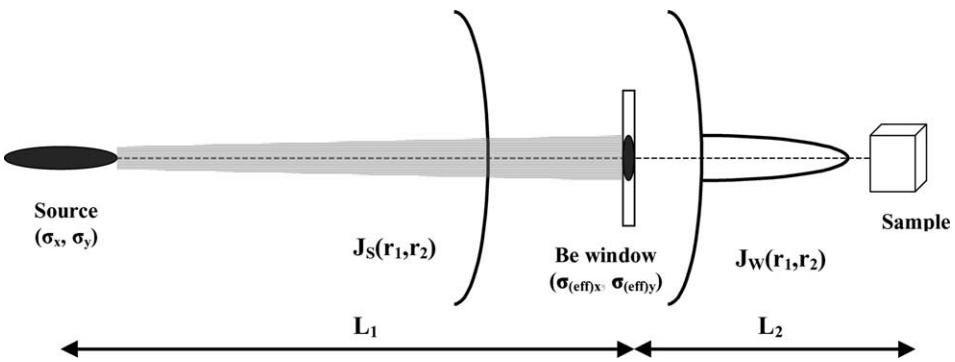

Fig. 3. Schematic view of propagation of the MIF from the incoherent synchrotron source through a random optical element (here Be window). Upon passing the Be window, the MIF has two components: one broad component with high coherency properties propagating directly from the source and a second one originating from the Be window that gives reduced coherence lengths at the sample position.

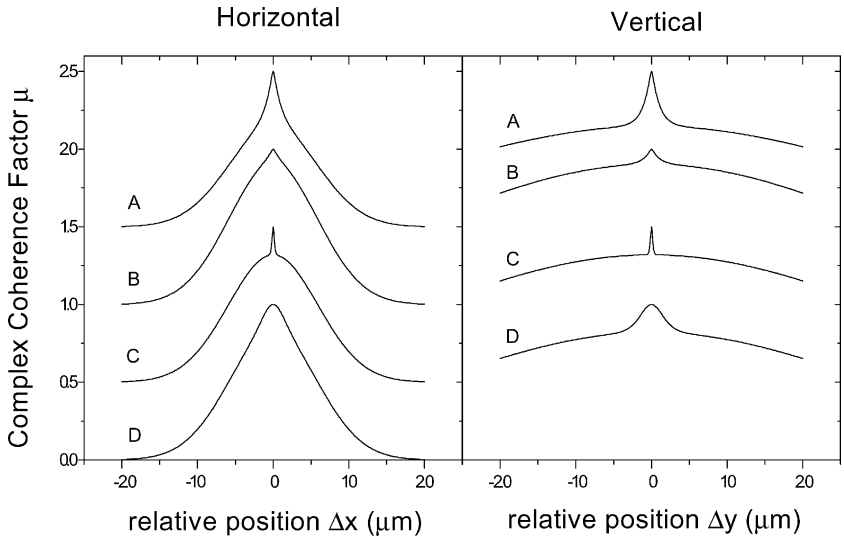

Fig. 4. Horizontal and vertical components of the complex coherence factor $\mu(\Delta x, \Delta y)$ calculated for the X-ray radiation with the wavelength $\bar{\lambda} = 1.5$ Å propagating through a random phase optical element at a distance $L_2 = 6$ m in front of the sample. Parameters of the source and statistical properties of an element are given in the text and are summarized in Table 1. Each curve is shifted by one unit for clarity.

are summarized in Table 1. Variance $\sigma_\Phi^2 = 0.5$ would correspond to the physical roughness of Be window σ_d about micron for 8 keV X-rays.

Curves A represent what we consider to be typical parameters for optics used in a CXD experiment at APS. Curves B represent a reduction of roughness variance. This improvement in the optics quality enhances the contribution of the broad component and at the same time reduces the sharp component contribution. Curves C reduce the correlation length of the roughness and as a result this immediately reduces the coherence length of the sharp component. Curves D show the improvement of coherency properties of the beam obtained by restricting the size of the beam at the position of an optical element.

Table 1
Parameters used for the calculation of the CCF $\mu(\Delta x, \Delta y)$ at the sample position

	σ_x (μm)	σ_y (μm)	$\sigma_{(\mathrm{eff})x,y}$ (mm)	σ_Φ^2	τ (μm)
A	250	50	1.5	0.5	1
B	250	50	1.5	0.1	1
C	250	50	1.5	0.5	0.1
D	250	50	0.15	0.5	1

Notations A–D are maintained throughout the paper, notably in Figs. 4 and 6. Here, $\sigma_{x,y}$ are the horizontal and vertical source sizes, $\sigma_{(\mathrm{eff})x,y}$ are an effective source size of the beam on the Be window, σ_Φ^2 and τ are variance and longitudinal correlation length of this window.

6. Effects of the optical element on the imaging of small crystals

In this part we will apply results obtained in the previous sections to a specific type of CXD experiment – coherent X-ray scattering from small crystalline particles [16]. Applying special iteration techniques originally proposed by Gerchberg and Saxton [47] and then further developed by Fienup [48] and Millane and Stroud [49], the intensity distribution obtained in such experiment can be inverted to give a real space image of the particle itself. It was demonstrated in our previous work [19] how the reconstructed shape can become modified by the coherency properties of the beam. Computer simulations showed that in the pure coherent beam the shape of the particle can be

reconstructed identically with the initially generated shape. However, reduced coherence of the beam can cause a region of high intensity to appear in the reconstructed image. We will see now how the two-component MIF discussed in the previous sections can modify the reconstructed image of the crystalline particle in CXD experiment.

We will assume below that quasi-monochromatic conditions are satisfied which means that in this kind of experiment time delays for X-ray propagation in a sample $\Delta\tau$ are much less than coherence times $\Delta\tau \ll \tau_c = l_c/c$. It was shown in [19] that in this situation the intensity diffracted from a small crystalline particle in the far-field limit under exact Bragg condition can be written as

$$I(\mathbf{Q}) = \int\int \mathrm{d}\mathbf{r}_1\,\mathrm{d}\mathbf{r}_2 s_z(\mathbf{r}_1)s_z(\mathbf{r}_2)\overline{J} \times (\mathbf{r}_1,\mathbf{r}_2)\,\mathrm{e}^{-\mathrm{i}\mathbf{Q}(\mathbf{r}_2-\mathbf{r}_1)}. \tag{61}$$

Here, $s_z(\mathbf{r}) = \int \mathrm{d}z s(\mathbf{r},z)$ is the projection of the shape function $s(\mathbf{r},z)$ of the particle, z axis is taken along the direction of the diffracted beam, and $\mathbf{r}$ is a 2D coordinate frame perpendicular to this direction. In the simplest case, the shape function $s(\mathbf{r},z)$ is defined equal to one inside the particle and to zero outside. For the exact Bragg condition the scattering vector $\mathbf{Q}$ is equal to $\mathbf{Q} = (\overline{k}/L)\mathbf{v}$, where $\mathbf{v}$ is the coordinate on the CCD detector located at a distance L from the sample perpendicular to the incoming beam. The beam illuminating the crystalline sample is assumed partially coherent with its MIF $\overline{J}(\mathbf{r}_1,\mathbf{r}_2)$.

We have shown in the previous sections that the coherency properties of the beam from the undulator source on the way to the sample can essentially change due to rescattering by imperfections of the Be windows and mirrors. According to (31)–(33), the MIF $\overline{J}(\mathbf{r}_1,\mathbf{r}_2)$ arriving at the sample can be written in a quite general way as a sum of two contributions with two different coherence lengths

$$\overline{J}(\mathbf{r}_1,\mathbf{r}_2) = C_1 J_{\mathrm{S}}(\mathbf{r}_1,\mathbf{r}_2) + C_2 J_{\mathrm{W}}(\mathbf{r}_1,\mathbf{r}_2).$$

Here, $J_{\mathrm{S}}(\mathbf{r}_1,\mathbf{r}_2)$ is a MIF (32) propagating along beamline from the source to the sample without rescattering and typically having large coherence lengths at the sample position. The second part $J_{\mathrm{W}}(\mathbf{r}_1,\mathbf{r}_2)$ (33) is a result of rescattering from all imperfections of windows or mirrors and has reduced coherence length. In a simple beamline set up (Fig. 2) with one optical element on the way from the source to the sample both parts of the incoming MIF $\overline{J}(\mathbf{r}_1,\mathbf{r}_2)$ (31) can be calculated according to the theory presented in the previous sections. Now taking into account that in the typical CXD experiment the size of the sample is of the order of microns, we can neglect any intensity variations in the incoming beam across the sample giving a good approximation

$$\begin{aligned} J_{\mathrm{S}}(\mathbf{r}_1,\mathbf{r}_2) &\simeq I_{\mathrm{S}}(0)\mu_{\mathrm{S}}(\Delta\mathbf{r}),\\ J_{\mathrm{W}}(\mathbf{r}_1,\mathbf{r}_2) &\simeq I_{\mathrm{W}}(0)\mu_{\mathrm{W}}(\Delta\mathbf{r}), \end{aligned} \tag{62}$$

where $I_{\mathrm{S}}(0)$ and $I_{\mathrm{W}}(0)$ are intensity values in the center of the incoming beam and $\mu_{\mathrm{S}}(\Delta\mathbf{r}), \mu_{\mathrm{W}}(\Delta\mathbf{r})$ are the normalized CCFs. Here, we want to note that in the case of small variance $\sigma_\Phi^2 \ll 1$ the intensity distribution $I_{\mathrm{W}}(0) \propto \sigma_\Phi^2$ according to (52) and (55). Substituting now (62) into (31) we get for the MIF of the incoming beam

$$\overline{J}(\Delta\mathbf{r}) = C_1 I_{\mathrm{S}}(0)\Big[\mu_{\mathrm{S}}(\Delta\mathbf{r}) + \widetilde{C}\mu_{\mathrm{W}}(\Delta\mathbf{r})\Big], \tag{63}$$

where $\widetilde{C} = C_2 I_{\mathrm{W}}(0)/[C_1 I_{\mathrm{S}}(0)]$ is a constant parameter that determines the contribution of the second term to the total MIF. To model the effects of decoherence introduced by the optical element we used expression (63) to fit the results of the exact near-field calculations of the MIF passing a random optical element made in the previous section (Fig. 4) with a simple functional form. The first CCF $\mu_{\mathrm{S}}(\Delta\mathbf{r})$, naturally, can be taken in the form of the Gaussian function (36) with coherence lengths $\xi_{\mathrm{S}x,y}$ (37). We found that a good approximation for the second CCF $\mu_{\mathrm{W}}(\Delta\mathbf{r})$ in the near-field corresponding to the four configurations of Table 1 was obtained either in the form of the Lorentzian function

$$\mu_{\mathrm{W}}(\Delta\mathbf{r}) = \frac{1}{1+(\Delta x/\xi_{\mathrm{W}x})^2}\,\frac{1}{1+(\Delta y/\xi_{\mathrm{W}y})^2} \tag{64}$$

or a Gaussian function with the coherence lengths $\xi_{\mathrm{W}x,y}$. Results of this fitting are summarized in

Table 2
Transverse coherence lengths of the "broad" ξ_S and "sharp" ξ_S components of the MIF $J_{in}(\Delta\mathbf{r})$ on the sample position obtained as a result of fitting with expression (63)

	ξ_{Sx} (μm)	ξ_{Sy} (μm)	$\xi_{Wx,y}$ (μm)	$\widetilde{C}$	$\sigma_{Qx,y}$ (μm^{-1})
A	5.92	29.6	0.8 (L)	0.545	1.25
B	5.92	29.6	0.8 (L)	0.11	1.25
C	5.92	29.6	0.15 (G)	0.22	6.67
D	5.92	29.6	1.5 (G)	0.22	0.67

Letters (L) and (G) mean Lorentzian or Gaussian form of CCF $\mu_W(\Delta\mathbf{r})$. Parameter $\sigma_{Qx,y}$ gives the size of distribution of incoherent intensity in the reciprocal space according to Eq. (73).

the Table 2. Letters (L) and (G) in Table 2 mean Lorentzian or Gaussian form of CCF $\mu_W(\Delta\mathbf{r})$. The MIF $\overline{J}(\mathbf{r}_1,\mathbf{r}_2)$ (63) with parameters listed in Table 2 is presented in Fig. 6(a). Parameter sets A–D correspond to the four configurations listed in Table 1 and Fig. 4.

The crystal shape was taken in the form of a uniform crystal with (1 1 1) facets shown in Fig. 5. The diffraction pattern from this crystal shape and reconstructed image of this crystal in the case of perfect coherent incoming beam are also shown in Fig. 5. The intensity distribution in the diffraction pattern has high contrast. The reconstructed shape of the particle for the coherent illumination conditions is identical to the initial one.

The diffraction patterns from the same crystal with the four different MIFs listed in Table 2 were calculated according to Eq. (61) and are presented in Fig. 6(b). From this figure we can see how the diffraction pattern is sensitive to different coherency properties of the incoming beam. A sharp component in the MIF smears the contrast in the central part of the diffraction pattern and in some cases reduces the visibility of the fringes. This is particularly apparent in Fig. 6(c). However in other cases, that are more often observed in experiment, the sharp component of the MIF affects only the small central part of the intensity distribution keeping high visibility for the range of higher $\mathbf{Q}$ values (Fig 6(b), image B).

We have applied the reconstruction algorithm discussed in detail in our previous work [19] to reconstruct the shape of the particle from the intensity distributions shown in Fig 6(b). No information about the partial coherence was included in the calculations, which are therefore not expected to converge perfectly. Results of this reconstruction are shown in Fig. 6(c). The left and right halves correspond to best reconstructions starting with different sets of random phases to give an impression of the reproducibility. As it is well seen from these results, different types of MIF give different results for the reconstructed shape of the particle. We can also observe that reduced coherence of the incoming beam affects the reproducibility of image reconstruction. The two general features introduced by the partial coherence are the sharp bright peak in the center of the image and the smearing of the borders of the particle. The same behavior was observed in reconstruction of the shape of gold particles from their diffraction pattern in CXD experiment [17]. We can see that fine features can be different for the two different sets of starting phases but general features as the smeared shape of the particle and the size of the "hot" spot are preserved. Better reconstruction images are obtained in the situation when the quality of the optical element is improved, in example B by reducing the rms roughness σ_ϕ, and in D by the introduction of a smaller aperture σ_{eff}.

The reconstructed images are mostly affected when the incoming MIF contains a very narrow sharp component (in our test calculations with $\xi_{Wx,y} = 0.15$ μm). This is the case of short correlation lengths τ on the element. As one can see in Fig. 6(c) (image C) the reconstructed image in this case produces a narrow high intensity region, smeared borders of the particle itself and even regions with zero density inside the particle. Improvement of the beam coherence by reducing the aperture on the optical element (Fig. 6(c), image D) can improve the quality of reconstructed image in the central part (enlarging the size of the bright peak) but still fails to produce correct shape of the crystal. For crystals of smaller sizes this improvement can be enough to reconstruct the correct shape of the particle.

In order to understand results of calculations qualitatively, we can calculate intensity distribu-

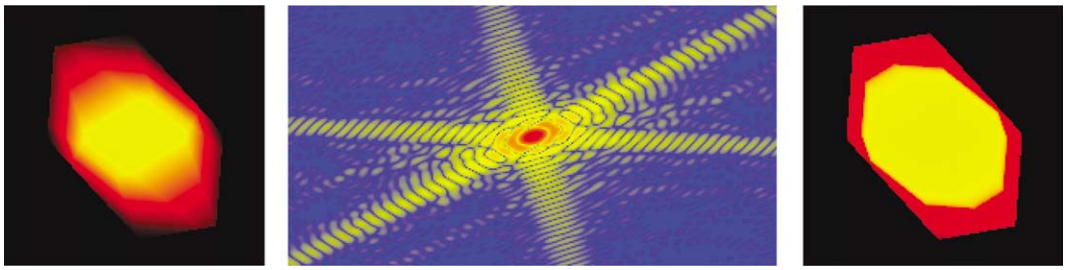

Fig. 5. Initial crystal shape (left image) used for calculations, its diffraction pattern (central image) in a perfect coherent beam and reconstructed shape of the particle (right image). Another non-linear color gradient is used for reconstructed image to enhance the background contribution. Calculations used an array of 700×400 pixels. In the figure, real space images have been cut to a size of 160×160 pixels and reciprocal space image to 300×160 pixels. The support region in the calculations was a rectangular box with a lateral size of 150×150 pixels.

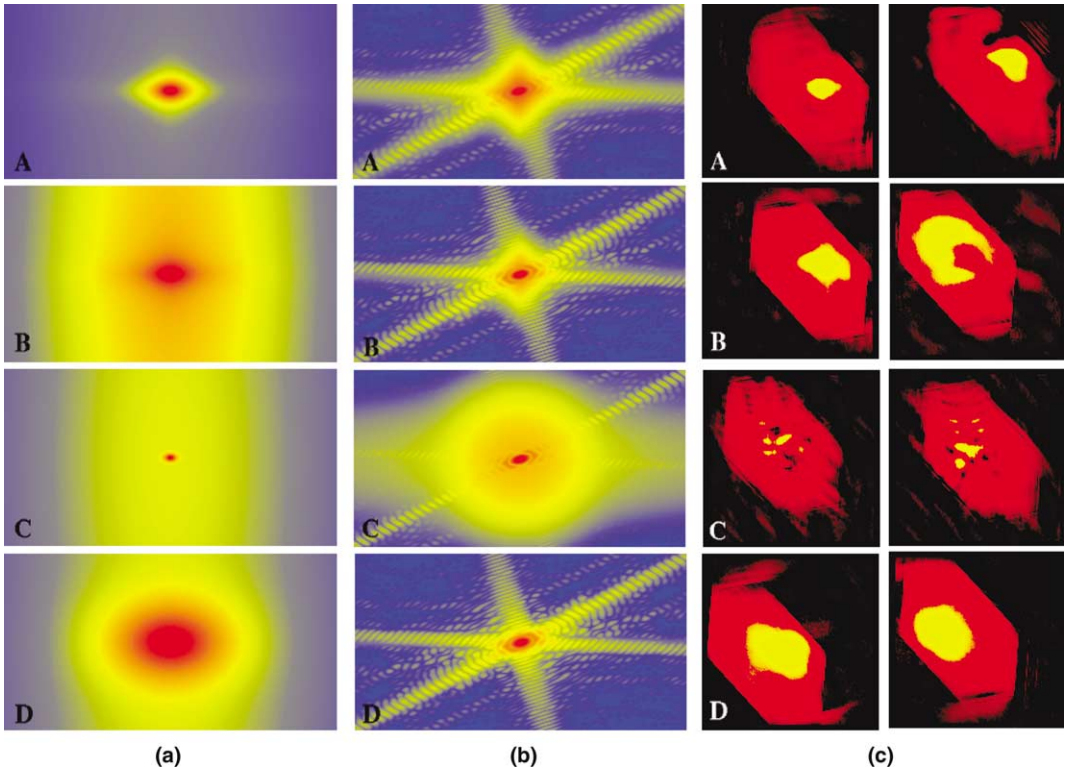

Fig. 6. The MIF (a) used for calculation of diffraction intensity patterns (b) from the crystal shape shown in Fig. 5. Reconstructed real-space images for two different sets of starting random phases are shown in (c). Parameters used for calculations of the A–D MIF are listed in Table 2.

tion further with some reasonable approximations. We will assume that CCF's $\mu_S(\Delta\mathbf{r})$ and $\mu_W(\Delta\mathbf{r})$ entering into an expression for the incoming MIF (63) have different coherence lengths compared with the average size of the particle D

$$\xi_S \gg D, \quad \xi_W \ll D. \tag{65}$$

Now substituting expression for the incoming MIF (63) into (61), we get for the intensity distribution

$$I(\mathbf{Q}) = \int\int \mathrm{d}\mathbf{r}_1\,\mathrm{d}\mathbf{r}_2 s_z(\mathbf{r}_1)s_z(\mathbf{r}_2)\mu_S(\Delta\mathbf{r})\,\mathrm{e}^{-\mathrm{i}\mathbf{Q}\Delta\mathbf{r}} + \widetilde{C}\int\int \mathrm{d}\mathbf{r}_1\,\mathrm{d}\mathbf{r}_2 s_z(\mathbf{r}_1)s_z(\mathbf{r}_2)\mu_W(\Delta\mathbf{r})\,\mathrm{e}^{-\mathrm{i}\mathbf{Q}\Delta\mathbf{r}}, \tag{66}$$

where intensity distribution $I(\mathbf{Q})$ is normalized by the value $C_1 I_S(0)$. Introducing the autocorrelation function

$$\varphi_{11}^z(\mathbf{r}) = \int \mathrm{d}\mathbf{r}' s_z(\mathbf{r}')s_z(\mathbf{r}'+\mathbf{r}), \tag{67}$$

the intensity distribution (66) can be written as

$$I(\mathbf{Q}) = \int \mathrm{d}\mathbf{r}\varphi_{11}^z(\mathbf{r})\mu_S(\mathbf{r})\,\mathrm{e}^{-\mathrm{i}\mathbf{Q}\mathbf{r}} + \widetilde{C}\int \mathrm{d}\mathbf{r}\varphi_{11}^z(\mathbf{r})\mu_W(\mathbf{r})\,\mathrm{e}^{-\mathrm{i}\mathbf{Q}\mathbf{r}}. \tag{68}$$

Now, we can make use of relationships (65) in calculating these integrals taking into account that in the first integral CCF $\mu_S(\Delta\mathbf{r})$ is a slow varying function compared with the autocorrelation function $\varphi_{11}^z(\mathbf{r})$ while in the second, the opposite applies. This approximation gives for the intensity distribution

$$I(\mathbf{Q}) \simeq \mu_S(0)\int \mathrm{d}\mathbf{r}\varphi_{11}^z(\mathbf{r})\,\mathrm{e}^{-\mathrm{i}\mathbf{Q}\mathbf{r}} + \widetilde{C}\varphi_{11}^z(0)\times\int \mathrm{d}\mathbf{r}\mu_W(\mathbf{r})\,\mathrm{e}^{-\mathrm{i}\mathbf{Q}\mathbf{r}} = \alpha I_{\mathrm{coh}}(\mathbf{Q}) + \beta I_{\mathrm{incoh}}(\mathbf{Q}), \tag{69}$$

where $I_{\mathrm{coh}}(\mathbf{Q})$ and $I_{\mathrm{incoh}}(\mathbf{Q})$ represent coherent and incoherent terms of the intensity distribution

$$I_{\mathrm{coh}}(\mathbf{Q}) = |A(\mathbf{Q})|^2 = \left|\int \mathrm{d}\mathbf{r}s_z(\mathbf{r})\,\mathrm{e}^{-\mathrm{i}\mathbf{Q}\mathbf{r}}\right|^2, \qquad I_{\mathrm{incoh}}(\mathbf{Q}) = \int \mathrm{d}\mathbf{r}\mu_W(\mathbf{r})\,\mathrm{e}^{-\mathrm{i}\mathbf{Q}\mathbf{r}} \tag{70}$$

and α and β are constants. In the case of the scattering from a small crystalline particle, the first part gives a sharp interference diffraction pattern while the second one smears this pattern. One important result here is that incoherent part of the scattered intensity is just the Fourier transform of the CCF $\mu_W(\mathbf{r})$. That means that sharper is the distribution of $\mu_W(\mathbf{r})$ in real space the broader will be incoherent intensity $I_{\mathrm{incoh}}(\mathbf{Q})$ contribution in the diffracted intensity. This result was observed in our direct computer simulations (see Figs. 6(a) and (b)). We can estimate the size of incoherent intensity distribution for different forms of CCF $\mu_W(\mathbf{r})$. For example, Gaussian distribution will give

$$I_{\mathrm{incoh}}(\mathbf{Q}) = 2\pi\xi_{Wx}\xi_{Wx}\exp\left[-\frac{Q_x^2}{2\sigma_{Qx}^2} - \frac{Q_y^2}{2\sigma_{Qy}^2}\right], \tag{71}$$

and Lorentzian distribution (64) will give

$$I_{\mathrm{incoh}}(\mathbf{Q}) = \pi\xi_{Wx}\xi_{Wx}\exp\left[-\frac{|Q_x|}{\sigma_{Qx}} - \frac{|Q_y|}{\sigma_{Qy}}\right], \tag{72}$$

where in both cases the width of incoherent distribution is determined by parameter

$$\sigma_{Qx,y} = \frac{1}{\xi_{Wx,y}}. \tag{73}$$

For example, for transverse coherence lengths of the sharp component $\xi_{Wx,y} \simeq 0.1$ μm it gives for the typical size of the incoherent distribution $\sigma_{Qx,y} \simeq 10\ \mu\mathrm{m}^{-1}$. The values of the parameter $\sigma_{Qx,y}$ typical for our computer simulations are presented in Table 2.

According to Eqs. (69) and (70), we have two different limits for the incoherent component. If coefficient $\widetilde{C}$ is small, the contribution of incoherent component in the total intensity distribution is also small and inversion of Eq. (69) will give just the shape of the particle. In the opposite limit when coefficient $\widetilde{C}$ is big, inversion of Eq. (69) will give, according to (70), the shape of CCF $\mu_W(\mathbf{r})$.

As a summary we can see from these test calculations that in order to produce high quality images of crystalline particles it is important to reduce the contribution to the MIF coming from the rescattered radiation from inhomogeneities of the Be windows and roughness of the mirrors. This can be achieved, for example, by special polishing of mirrors [40] and Be windows or slightly reducing the aperture of the incoming beam at the location of the optics.

Another important result, suggested by our analysis, is a way of filtering the experimental data in order to obtain images of higher quality. If the limit (65) applies, then filtering can be obtained just by subtracting the incoherent background in the form of estimates of the functions $I_{\mathrm{incoh}}(\mathbf{Q})$ (71) and (72). If conditions (65) are violated, then the general form of the intensity distribution (61) with

MIF in the form of the two-component function (31) must be used for filtering the measured data.

7. Conclusions

In conclusion we have seen how coherency properties of the X-ray beam can change while propagation through optics present in a typical hard X-ray beamline. It was shown that it is convenient to describe coherency properties of the beam by the MIF which can be obtained through Eq. (11). Detailed knowledge of the structure of an optical element, given by its transmittance function $T(\mathbf{u})$, is necessary to calculate the coherency properties of the beam. Limits of coherent and incoherent illumination of an element were discussed.

It was then shown that in the situation that is often met in practice when the effective size of the beam incoming on the optical element is much bigger than its coherence length, this element can be treated as a random optical element described by its statistical properties: variance σ_ϕ^2 and correlation length τ. It was shown that for this random element the MIF $\overline{J}(\mathbf{r}_1,\mathbf{r}_2)$ propagating through such optics and incoming on the sample will split into two parts. The first part $J_S(\mathbf{r}_1,\mathbf{r}_2)$ describes propagation of radiation directly from incoherent source to the sample and has large coherence lengths, however the second part $J_W(\mathbf{r}_1,\mathbf{r}_2)$ that results from rescattering of radiation by inhomogeneities of the optics is responsible for the decoherence of the original beam and has reduced coherence lengths. The contribution of the second term in MIF $\overline{J}(\mathbf{r}_1,\mathbf{r}_2)$ depends on the quality of an optics through its roughness and correlation of fluctuations. It can be reduced by the special preparation of the windows and mirrors (e.g., by polishing) or by taking smaller grazing angles θ for the mirrors. The properties of this second part of MIF were discussed both in the far-field as well as in the near-field limit. It was shown that for the typical configuration of a beamline, in which the last element is usually an exit Be window, far-field conditions are violated and near-field analysis is important. It is interesting to note here that similar two-component MIF was measured in the recent experiments on APS [34].

In the last section we discussed how this two-component MIF can influence the intensity distribution obtained in a CXD experiment on nanoparticles. It was shown that images obtained by inversion of this intensity distribution can contain some features (regions of high intensity or even zero density) that can be associated with partial coherence of the beam rather then present in particle itself.

Analysis given in this paper can be useful for the estimates of the coherency properties of existing X-ray beamlines in the experiments that utilize coherence and also for the new constructed beamlines dedicated for experiments that need to preserve coherence.

Acknowledgements

We acknowledge useful and stimulating discussions with K. Nugent, S. Sinha and M. Sutton. This work was supported by NSF DMR98-76610 and US Department of Energy under DEFG02-91ER45439.

Appendix A. Calculation of undistorted part of MIF $J_S(\mathbf{r}_1,\mathbf{r}_2)$

We will show now that in the case of an incoherent source at distance L_1 from the random optical element, the MIF $J_S(\mathbf{r}_1,\mathbf{r}_2)$ at the sample position can be written as directly propagating from this incoherent source.

Assuming that synchrotron radiation from the bending magnet or an insertion device can be well approximated as an incoherent source of radiation, the corresponding CCF $\mu(\mathbf{s}_1,\mathbf{s}_2)$ can be taken in the form of the delta-function $\mu(\mathbf{s}_2-\mathbf{s}_1)=\kappa\delta(\mathbf{s}_2-\mathbf{s}_1)$, where κ is the numerical constant with the dimension of the length squared [37,38]. In this limit the MIF of the source can be written as $J(\mathbf{s}_2-\mathbf{s}_1)=\kappa I_S(\mathbf{s})\delta(\mathbf{s}_2-\mathbf{s}_1)$, where $I_S(\mathbf{s})$ is the intensity distribution of incoherent source. Using the propagation law for the MIF (5) in the paraxial approximation, the MIF incoming on the Be window from this incoherent synchrotron source can be written as

$$J_{\mathrm{in}}(\mathbf{u}_1,\mathbf{u}_2)=\kappa\int I_{\mathrm{S}}(\mathbf{s})P_{L_1}(\mathbf{u}_1-\mathbf{s})\times P^{*}_{L_1}(\mathbf{u}_2-\mathbf{s})\,\mathrm{d}\mathbf{s}, \tag{A.1}$$

where the definition of Green's functions (12) was used and one integral was taken using the properties of the δ-function. Now substituting this expression into Eq. (32) calculated at the sample position, we obtain

$$J_{\mathrm{S}}(\mathbf{r}_1,\mathbf{r}_2)=\kappa\int\int\int I_{\mathrm{S}}(\mathbf{s})P_{L_1}(\mathbf{u}_1-\mathbf{s})P^{*}_{L_1}(\mathbf{u}_2-\mathbf{s})\times P_{L_2}(\mathbf{r}_1-\mathbf{u}_1)P^{*}_{L_2}(\mathbf{r}_2-\mathbf{u}_2)\,\mathrm{d}\mathbf{s}\,\mathrm{d}\mathbf{u}_1\,\mathrm{d}\mathbf{u}_2. \tag{A.2}$$

Using the properties of the Fourier transform it is easy to show that the propagator function obeys the following convolution theorem [50]:

$$\int P_{L_1}(\mathbf{u}-\mathbf{s})P_{L_2}(\mathbf{r}-\mathbf{u})\,\mathrm{d}\mathbf{u}=P_{L_1+L_2}(\mathbf{r}-\mathbf{s}).$$

Performing now integration in (A.2) over $\mathbf{u}_1,\mathbf{u}_2$, we obtain

$$J_{\mathrm{S}}(\mathbf{r}_1,\mathbf{r}_2)=\kappa\int I_{\mathrm{S}}(\mathbf{s})P_{L_1+L_2}(\mathbf{r}_1-\mathbf{s})P^{*}_{L_1+L_2}(\mathbf{r}_2-\mathbf{s})\,\mathrm{d}\mathbf{s}. \tag{A.3}$$

This is an important result showing that MIF $J_{\mathrm{S}}(\mathbf{r}_1,\mathbf{r}_2)$ at the sample position can be calculated directly from the intensity distribution $I_{\mathrm{S}}(\mathbf{s})$ of the source on the distance L_1+L_2 without any influence of an optical element (Be window or a mirror).

Substituting now in expression for the MIF $J_{\mathrm{S}}(\mathbf{r}_1,\mathbf{r}_2)$ (A.3) an explicit form of the Green's functions $P_{L_1+L_2}(\mathbf{r}-\mathbf{s})$ (12), we obtain

$$J_{\mathrm{S}}(\mathbf{r}_1,\mathbf{r}_2)=\kappa\frac{\mathrm{e}^{-\mathrm{i}\psi_{\mathrm{S}}}}{[\overline{\lambda}(L_1+L_2)]^2}\int_{\Sigma}I_{\mathrm{S}}(\mathbf{s})\times\exp\left[\mathrm{i}\frac{\overline{k}}{L_1+L_2}(\mathbf{r}_2-\mathbf{r}_1)\mathbf{s}\right]\mathrm{d}\mathbf{s}, \tag{A.4}$$

where $\psi_{\mathrm{S}}=\overline{k}/[2(L_1+L_2)](\mathbf{r}_2^2-\mathbf{r}_1^2)$. This expression is well known as van Cittert–Zernike theorem [37,38] and gives coherency properties of the beam from an incoherent source on the distance L_1+L_2.

To the extent that the intensity distribution for the synchrotron radiation source can be approximated by a Gaussian function (35), Eq. (A.4) gives for the MIF

$$J_{\mathrm{S}}(\mathbf{r}_1,\mathbf{r}_2)=\kappa\frac{2\pi\sigma_x\sigma_y I_0}{[\overline{\lambda}(L_1+L_2)]^2}\,\mathrm{e}^{-\mathrm{i}\psi_{\mathrm{S}}}\times\exp\left[-\frac{\Delta x^2}{2\xi^2_{\mathrm{S}x}}-\frac{\Delta y^2}{2\xi^2_{\mathrm{S}y}}\right], \tag{A.5}$$

where

$$\xi_{\mathrm{S}x,y}=\frac{L_1+L_2}{\overline{k}\sigma_{x,y}} \tag{A.6}$$

are transverse coherence lengths on the sample position given by the size of the incoherent source $\sigma_{x,y}$ and the distance from the source to the sample L_1+L_2.

References

[1] T. Thurn-Albrecht, G. Meier, P. Müller-Buschbaum, A. Patkowski, W. Steffen, G. Grübel, D.L. Abernathy, O. Diat, M. Winter, M.G. Koch, M.T. Reetz, Phys. Rev. E 59 (1999) 642.

[2] S.G.J. Mochrie, A.M. Mayes, A.R. Sandy, M. Sutton, S. Brauer, G.B. Stephenson, D.L. Abernathy, G. Grübel, Phys. Rev. Lett. 78 (1997) 1275.

[3] O.K.C. Tsui, S.G.J. Mochrie, Phys. Rev. E 57 (1998) 2030.

[4] D.O. Riese, W.L. Vos, G.H. Wegdam, F.G. Poelwijk, G. Grübel, D.L. Abernathy, Phys. Rev. E 61 (2000) 1676.

[5] T. Seydel, A. Madsen, M. Tolan, G. Grübel, W. Press, Phys. Rev. B 63 (2001) 0734099(4).

[6] I. Sikharulidze, I.P. Dolbnya, A. Fera, A. Madsen, B. Ostrovskii, W. de Jeu, Phys. Rev. Lett. 88 (2002) 115503(4).

[7] A. Snigirev, I. Snigireva, V. Kohn, S. Kuznetsov, I. Schelokov, Rev. Sci. Instrum. 66 (1995) 5486.

[8] S.W. Wilkins, T.E. Gureyev, D. Gao, A. Pogany, A.W. Stevenson, Nature 384 (1996) 335.

[9] T.E. Gureyev, C. Raven, A. Snigirev, I. Snigireva, S.W. Wilkins, J. Phys. D 32 (1999) 563.

[10] P. Cloetens, W. Ludwig, J. Baruchel, D. Van Dyck, J. Van Landuyt, J.P. Guigay, M. Schlenker, Appl. Phys. Lett. 75 (1999) 2912.

[11] J. Miao, P. Charalambous, J. Kirz, D. Sayre, Nature (London) 400 (1999) 342.

[12] I.K. Robinson, J.L. Libbert, I.A. Vartanyants, J.A. Pitney, D.M. Smilgies, D.L. Abernathy, G. Grübel, Phys. Rev. B 60 (1999) 9965.

[13] J.A. Pitney, I.K. Robinson, I.A. Vartanyants, R. Appelton, C.P. Flynn, Phys. Rev. B 62 (2000) 13084.

[14] A. Letoublon, F. Yakhou, F. Livet, F. Bley, M. de Boissieu, L. Mancini, R. Caudron, C. Vettier, J. Gastaldi, Europhys. Lett. 54 (2001) 753.

[15] B. Lengeler, Naturwissenschaften 88 (2001) 249.

[16] I.K. Robinson, I.A. Vartanyants, G.J. Williams, M.A. Pfeifer, J.A. Pitney, Phys. Rev. Lett. 87 (2001) 195505(4);

G.J. Williams, M.A. Pfeifer, I.A. Vartanyants, J.K. Robinson, Phys. Rev. Lett. 90 (2003) 175501 (4).
[17] A.C. Kak, M. Slaney, Principles of Computerized Tomographic Imaging, Society of Industrial and Applied Mathematics, Philadelphia, 2001.
[18] I.K. Robinson, I.A. Vartanyants, Appl. Surf. Sci. 182 (2001) 186.
[19] I.A. Vartanyants, I.K. Robinson, J. Phys. 13 (2001) 10593.
[20] S.K. Sinha, M. Tolan, A. Gibaud, Phys. Rev. B 57 (1998) 2740.
[21] J. Borowski, J. Gronkowski, J. Phys. D 34 (2001) 3496.
[22] A. Szöke, Acta Cryst. A 57 (2001) 586.
[23] M. Born, E. Wolf, Principles of Optics, seventh ed., Cambridge University Press, Cambridge, 1999.
[24] J.E. Trebes, K.A. Nugent, S. Mrowka, R.A. London, T.W. Barbee, M.R. Carter, J.A. Koch, B.J. MacGowan, D.L. Matthwes, L.B. Da Silva, G.F. Stona, M.D. Feit, Phys. Rev. Lett. 68 (1992) 588.
[25] Y. Takayama, R.Z. Tai, T. Hatano, T. Miyahara, W. Okamoto, Y. Kagoshima, J. Synchrotron. Rad. 5 (1998) 456.
[26] Y. Takayama, T. Hatano, T. Miyahara, W. Okamoto, J. Synchrotron. Rad. 5 (1998) 1187.
[27] K. Tamasaku, T. Ishikawa, Acta Cryst. A 57 (2001) 197.
[28] K. Fezzaa, F. Comin, S. Marchesini, R. Coisson, M. Belakhovsky, J. X-ray Sci. Technol. 7 (1997) 12.
[29] P. Cloetens, J.P. Guigay, C. De Martino, J. Baruchel, M. Schlenker, Opt. Lett. 22 (1997) 1059.
[30] B. Lin, M.L. Schlossman, M. Meron, S.M. Williams, Z. Huang, P.J. Viccaro, Phys. Rev. B 58 (1998) 8025.
[31] V. Kohn, I. Snigireva, A. Snigirev, Phys. Rev. Lett. 85 (2000) 2745;
Opt. Commun. 198 (2001) 293.
[32] M. Yabashi, K. Tamasaku, T. Ishikawa, Phys. Rev. Lett. 87 (2001) 140801(4).
[33] D. Paterson, B.E. Allman, P.J. McMahon, J. Lin, N. Moldovan, K.A. Nugent, I. McNulty, C.T. Chantler, C.C. Retsch, T.H.K. Irving, D.C. Mancini, Opt. Commun. 195 (2001) 79.
[34] J. Lin, D. Paterson, A.G. Peele, P.J. McMahon, C.T. Chantler, K.A. Nugent, B. Lai, N. Moldovan, Z. Cai, D.C. Mancini, I. McNulty, Phys. Rev. Lett. 90 (2003) 074801(4).
[35] A. Souvorov, M. Yabashi, K. Tamasaku, T. Ishikawa, Y. Mori, Yamauchi, K. Yamamura, A. Saito, J. Synchrotron. Rad. 9 (2002) 223.
[36] A. Snigirev, I. Snigireva, V. Kohn, S.M. Kuznetsov, Nucl. Instrum. Meth. A 370 (1996) 634.
[37] J.W. Goodman, Statistical Optics, Wiley, New York, 1985.
[38] L. Mandel, E. Wolf, Optical Coherence and Quantum Optics, Cambridge University Press, Cambridge, 1995.
[39] S.K. Sinha, E.B. Sirota, S. Garoff, H.B. Stanley, Phys. Rev. B 38 (1988) 2297.
[40] Y. Mori, K. Yamauchi, K. Yamamura, Y. Sano, Rev. Sci. Instrum. 71 (2000) 4620.
[41] I.K. Robinson, C.A. Kenney-Benson, I.A. Vartanyants, Recent experiments on APS source have shown that the typical particle size on Be window is about 1 μm, Physica B, Proceedings of SXNS-7 Conference (in press).
[42] A detailed description can be found, for example, in [43] (vols. 1, 2 and 3). For a good overview of the elements of the theory of probability see also [37] (Chapters 2 and 3) and [38] (Chapters 1 and 2).
[43] S.M. Rytov, Yu.A. Kravtsov, V.I. Tatarskii, Principles of Statistical Radiophysics, Springer, Berlin, Heidelberg, New York, 1987.
[44] R.J. Dejus, B. Lai, E.R. Moog, E. Gluskin, Argonne National Laboratory Technical Bulletin ANL/APS/TB-17, 1994;
H.M. Bizek, Argonne National Laboratory Technical Bulletin ANL/APS/TB-26, 1996. Improvements of the synchrotron source have since reduced the horizontal size of the source from $\sigma_x \simeq 350$ μm published in these reports to present number $\sigma_x \simeq 250$ μm that is used in our calculations.
[45] See, for example, in J. Als-Nielsen, D. McMorrow, Elements of Modern X-ray Physics, Wiley, New York, 2001.
[46] The value of constant I_0^{in} depend on the optics upstream the random optic element. For the Gaussian source and beamline with one optical element (Fig. 2) from (34) to (35) $I_0^{\text{in}} = 2\pi\kappa\sigma_x\sigma_y I_0/(\lambda L_1)^2$.
[47] R.W. Gerchberg, W.O. Saxton, Optik 35 (1972) 237.
[48] J.R. Fienup, Appl. Opt. 21 (1982) 2758.
[49] R.P. Millane, W.J. Stroud, J. Opt. Soc. Am. A 14 (1997) 568.
[50] V. Kohn, Phys. Scripta 56 (1997) 14.